MODE INTERACTIONS OF AN INCLINED CABLE EXCITED CLOSE TO ITS SECOND NATURAL FREQUENCY

V. TZANOV*, B. KRAUSKOPF†, S.A. NEILD‡, AND D.J. WAGG‡

Abstract. In a cable-stayed bridge the bridge deck is supported by a large number of inclined cables of varying lengths and inclinations, which are suspended from a bridge tower. Vertical excitation of the bridge deck, for example, due to traffic loading, is influencing the cables. This may result in quite complex dynamics of those cables, whose basic vibration modes are near resonances with the excitation. These dynamics are nonlinear due to gravitational sag and tension variations in the cable.

We consider here a single inclined cable of length L, whose lower support is periodically excited in the vertical direction with a frequency that is close to the second natural frequency ω_2 of the cable. This system is described mathematically by a system of six ordinary differential equations for the contributions of three basic modes of vibration: the second in-plane mode (of vertical motion) and the first and second out-of-plane modes (of horizontal motion). The participating basic modes and the parameters are chosen to represent a scaled-down cable experiment that was designed to represent a full-scale cable of a realistic cable-stayed bridge.

More specifically, we present a comprehensive bifurcation study of the different possible coupled-mode responses of the cable, which are distinguished by which of the two out-of-plane modes participate in the dynamics apart from the directly excited in-plane mode. These coupled modes are equilibria of the ODE model, and they are continued numerically with the package AUTO in the dimensionless amplitude Δ/L and the frequency ratio Ω/ω_2 of the excitation. Each type of coupled-mode response, of which there are four, is computed and represented as a surface of equilibria in $(\Delta/L, \Omega/\omega_2, ||N||)$-space, where $||N||$ is a suitable norm. We also compute curves of bifurcations, along which the stability of the equilibria changes and different surfaces meet. Overall, we obtain a geometric picture of the two-parameter bifurcation diagram of the coupled-mode response of the cable. Chosen cross sections, for fixed Δ/L and for fixed Ω/ω_2, illucidate its intricate properties.

Key words. Cable dynamics, parametric excitation, modal equations, bifurcation analysis, equilibrium surfaces.

AMS subject classifications. 70K30, 70K50, 34C15

*DEPARTMENT OF ENGINEERING MATHEMATICS, UNIVERSITY OF BRISTOL, QUEEN'S BUILDING, UNIVERSITY WALK, BRISTOL BS8 1TR, UNITED KINGDOM

†DEPARTMENT OF MATHEMATICS, THE UNIVERSITY OF AUCKLAND, PRIVATE BAG 92019, AUCKLAND 1142, NEW ZEALAND

‡DEPARTMENT OF MECHANICAL ENGINEERING, UNIVERSITY OF BRISTOL, QUEEN'S BUILDING, UNIVERSITY WALK, BRISTOL BS8 1TR, UNITED KINGDOM

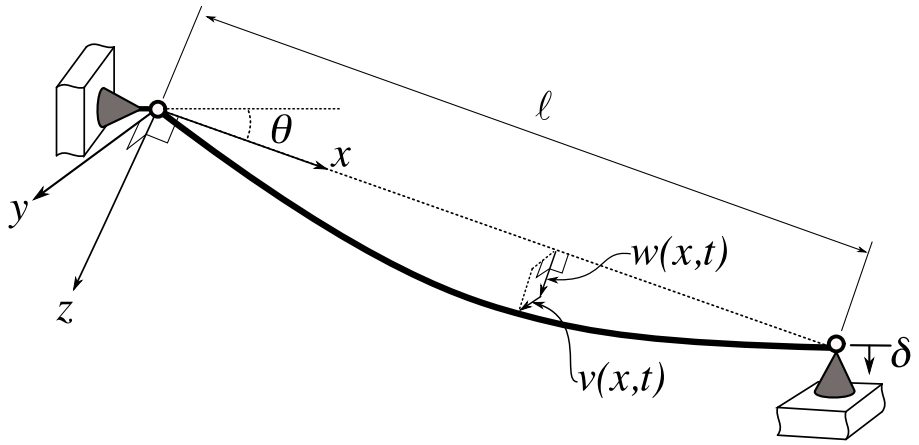

FIG. 1. *Schematic representation of an inclined cable with vertical input motion at the lower attachment point. Here $x \in [0, \ell]$, where ℓ is the support separation distance, θ is the angle of inclination, and δ is the support excitation; moreover, $v(x,t)$ and $w(x,t)$ are the out-of-plane (y-direction) and in-plane (z-direction) modal responses of the cable, respectively; see also [32, 33].*

1. INTRODUCTION. In a cable-stayed bridge, the towers support the deck by many inclined cables of different length [11]. Therefore, deck excitation due to traffic or other external forces can trigger harmonic vibrations of some of the cables. This motivates the need to explore the dynamic behaviour of inclined cables due to harmonic excitation, such as those present in cable-stayed bridges. Cable dynamics is nonlinear due to gravitational sag and tension variations during oscillations, and these nonlinearities result in the coupling between different basic modes of the cable. Interesting dynamic responses are the result of this coupling, in light of other important properties of the system:

(1) cables are very lightly damped;
(2) both in-plane (vertical) and out-of-plane (horizontal) motion is possible;
(3) the natural frequencies of the basic modes and/or the excitation may be close to resonance.

We consider here a single inclined cable subject to vertical excitation of its lower support; the corresponding physical setup is sketched in figure 1. It has been shown that small amplitude motion of the cable anchorage can result in large amplitude cable vibrations [16]. Parametric excitation was studied by using Mathieu-Hill equations [27, 30]; the most significant effect was shown to occur when the ratio between the excitation frequency and the first natural frequency of the cable is 2:1 [13]. Out-of-plane motion was considered in [8], where auto-parametric resonance and nonlinearities for the multiple cable modes are included. The coupling between the in-plane and out-of-plane modes of vibration of the cable was studied by using nonlinear Mathieu-type equations to model parametric resonance; see [5, 6, 7]. The triggering of an out-of-plane motion is also widely formulated as an instability of the semi-trivial solution (in which only the directly excited mode is present in the response) [2, 9, 14, 18, 19, 22, 24, 26]. Rich experimental analysis of the cable response in out-of-plane modes of vibration, periodic oscillations and even chaotic behaviour has been reported in [17, 20, 21, 23].

Warnitchai *et al.* [33] derived model equations of motion for the nonlinearly coupled basic modes of an inclined cable subject to support excitation; see [32] for an extended discussion of the derivation. A three-mode model based on Warnitchai's equations for the second in-plane mode and the first and second out-of-plane modes was considered in [9] These three second-order differential equations are scaled and averaged and led to a system of six autonomous ODEs. Their solutions

represent the coefficients that modulate the sine and cosine members in the mode shape functions of the cable response. In [9] these solutions were used to identify the boundary of the directly excited pure second in-plane response in a parameter plane via examination of the localised stability of each out-of-plane mode about its zero response; these results were validated with experimental data of a scaled model of an inclined cable. Generalised equations of the same type as those in [9] for excitation in every natural frequency and response in all possible modes are provided in [14]; there a theoretical and an experimental study are compared not only for excitation in the second natural frequency of the cable, but also for excitation its first, third and fourth natural frequency. A four-mode model based on Warnitchai's equations was investigated and verified experimentally in [15], where the response amplitudes of the various modes are studied and compared with experimental measurements for the cable discussed in [14].

In this paper we present a detailed bifurcation study of the three-mode ODE model from [9] to investigate when and how the two basic out-of-plane modes contribute to the dynamics upon the direct excitation of the second in-plane mode. We consider an inclined cable of length L with second natural frequency ω_2 (for both in-plane and out-of-plane vibrations) and excited vertically at its lower end by the periodic excitation $\delta = \Delta\cos(\Omega t)$. Steady-state solutions (equilibria) of the system of autonomous ODE correspond to periodic dynamics of the cable. The equilibria can be distinguished by determining which of the three basic in-plane and out-of-plane modes contribute to the cable response (i.e., have non-zero amplitudes); we refer to these equilibria as (coupled) modes of the cable. The different types of equilibria, and their bifurcations, are continued with the numerical continuation software AUTO [3, 4] in two parameters: the frequency ratio Ω/ω_2 and the dimensionless amplitude Δ/L. The equilibria, and hence the different types of modes, are represented by surfaces in $(\Omega/\omega_2, \Delta/L, ||N||)$-space by plotting the Euclidean norm $||N||$ of their amplitude contributions. Modes that are stable correspond to the observable dynamics of the cable, and they are distinguished by darker shading. Different surfaces meet or encounter changes of stability along curves of bifurcations that are also computed. In this way, we obtain a comprehensive geometric picture of surfaces of the different coupled modes of vibration. Its knowledge allows one to identify the contributions of the three basic in-plane and out-of-plane modes to the observed cable response for given (or changing) amplitude and frequency of the periodic excitation $\delta(t)$. This is illucidated with the discussion of one-parameter bifurcation diagrams at cross sections of interest.

The paper is organized as follows. The differential equation model of the cable, which describes the evolution of its three basic modes, are introduced in section 2 together with the specific settings of the parameters. Section 3 is devoted to the bifurcation analysis of the system as a function of frequency and amplitude of the excitation. The overall picture of connected surfaces of equilibria is built up gradually in sections 3.1–3.5 by adding surfaces corresponding to the different coupled modes of vibration one by one. One-parameter bifurcation diagrams as a function of the excitation frequency, which are intersections of the surfaces of equilibria for fixed amplitude of excitation, are considered in section 3.6. Finally, some conclusions are drawn in section 4.

2. Three-mode model of inclined cable dynamics. In this study we concentrate on sinusoidal support excitations $\delta(t)$ close to the second in-plane natural frequency of an inclined cable, as sketched in figure 1. We chose parameters to represent the cable that was experimentally tested in [9], which was designed as a scaled-down model for larger, realistic cable cable. The experiment used a 1.98m long, 0.8mm diameter steel cable, inclined at 20^o to the horizontal, with a mass of 0.67 kg/m (which is achieved by using a series of lead weights).

We consider here the dynamics of the directly excited second in-plane mode with natural frequency $\omega_2 = 2\omega_1$, and the first and second out-of-plane modes. These two out-of-plane modes are included as they have 2:1 and 1:1 internal resonances with the second in-plane mode (i.e., natural frequencies $\omega_1 = \omega_2/2$ and ω_2, respectively). The first in-plane mode, on the other hand,

is not included as its frequency is $1.07\omega_1$ (see [9]) and, therefore, exhibits a significant response only at excitation frequencies beyond those considered here; the inclusion of this basic mode in the model is discussed in [28] and [29].

The modal equations of motion that form the basis of this study were derived in their general form by Warnitchai *et al.* [33]; see also the discussion in [32]. When scaled and averaged (see [9] for the details) these equations give the following expressions for the amplitude dynamics of the modes:

$$
\begin{aligned}
y'_{1c} &= -\xi\omega_1 y_{1c} - \left(\mu\omega_1 + \frac{N_1\Delta}{4\omega_1} - \frac{3W_{12}}{32\omega_1}Y_1^2 - \frac{W_{12}}{4\omega_1}(Y_2^2+Z_2^2)\right)y_{1s}, \\
y'_{1s} &= \left(\mu\omega_1 - \frac{N_1\Delta}{4\omega_1} - \frac{3W_{12}}{32\omega_1}Y_1^2 - \frac{W_{12}}{4\omega_1}(Y_2^2+Z_2^2)\right)y_{1c} - \xi\omega_1 y_{1s}, \\
y'_{2c} &= \left(\frac{W_{12}z_{2c}z_{2s}}{2\omega_1} - 2\xi\omega_1\right)y_{2c} - \left(2\mu\omega_1 - \frac{W_{12}}{8\omega_1}\left(Y_1^2 + 6(Y_2^2+Z_2^2) - 4z_{2c}^2\right)\right)y_{2s}, \\
y'_{2s} &= \left(2\mu\omega_1 - \frac{W_{12}}{8\omega_1}\left(Y_1^2 + 6(Y_2^2+Z_2^2) - 4z_{2s}^2\right)\right)y_{2c} - \left(2\xi\omega_1 + \frac{W_{12}z_{2c}z_{2s}}{2\omega_1}\right)y_{2s}, \\
z'_{2c} &= \left(\frac{W_{12}y_{2c}y_{2s}}{2\omega_1} - 2\xi\omega_1\right)z_{2c} - \left(2\mu\omega_1 - \frac{W_{12}}{8\omega_1}\left(Y_1^2 + 6(Y_2^2+Z_2^2) - 4y_{2c}^2\right)\right)z_{2s}, \\
z'_{2s} &= \left(2\mu\omega_1 - \frac{W_{12}}{8\omega_1}\left(Y_1^2 + 6(Y_2^2+Z_2^2) - 4y_{2s}^2\right)\right)z_{2c} - \left(2\xi\omega_1 + \frac{W_{12}y_{2c}y_{2s}}{2\omega_1}\right)z_{2s} - B\Delta\omega_1.
\end{aligned}
\tag{2.1}
$$

Here z and y represent in-plane and out-of-plane modes, respectively, where subscripts 1 and 2 indicate the mode number and subscripts c and s indicate sine and cosine components of the response. The averaged amplitudes of the normalised second in-plane and the first and second out-of-plane modes are written as $Z_2 = \sqrt{z_{1c}^2 + z_{1s}^2}$, $Y_1 = \sqrt{y_{1c}^2 + y_{1s}^2}$ and $Y_2 = \sqrt{y_{2c}^2 + y_{2s}^2}$, respectively. Throughout we consider the norm

$$
||N|| = \frac{\sqrt{Z_2^2 + Y_1^2 + Y_2^2}}{L}, \tag{2.2}
$$

which represents the combined amplitude of the cable response associated with the (steady-state) solutions of (2.1).

The external lower support displacement excitation is $\delta = \Delta\cos(\Omega t)$, where Ω is chosen to be close to ω_2; therefore, a small detuning parameter μ defined as $\Omega = 2\omega_1(1+\mu)$ has been introduced. Moreover, the scaled time $\tau = (1+\mu)t$ has been used in (2.1) and $(\cdot)'$ denotes the derivative of $(\cdot)$ with respect to this scaled time.

We vary the normalized amplitude Δ/L and frequency Ω/ω_2 of the excitation as the continuation parameters. The other parameters are fixed to the values given in Table 1. Here, the damping ratio ξ is assumed to be the same for all three basic modes considered, which is in line with the experimental study in [9]. The parameters in Table 1 have been calculated for the specific cable under consideration from the relationships

$$
\begin{aligned}
&W_{nk} = \nu_{nk}/m, \quad N_n = 2\eta_n \sin\theta/m, \quad B = \zeta_2\cos\theta/m, \\
&E_q = \frac{1}{1+\lambda^2/12}E, \quad \lambda^2 = \frac{E}{\sigma_s}\left(\frac{\gamma\ell}{\sigma_s}\right)^2, \quad \gamma = \rho g\cos\theta, \\
&\nu_{nk} = \frac{EA\pi^4 n^2 k^2}{8\ell^3}, \quad \eta_n = \frac{E_q A\pi^2 n^2}{4\ell^2}, \quad \zeta_n = \frac{2m}{n\pi}, \quad \omega_n = \frac{n\pi}{L}\sqrt{\frac{\sigma_s}{\rho}}.
\end{aligned}
\tag{2.3}
$$

TABLE 1
Cable parameters and their values; note that B and ξ are nondimensional.

N_1 [Hz^2/m]	W_{12} [s^{-2}m^{-2}]	ω_1 [rad/s]	B	ξ
5.6×10^4	9.46×10^5	27.7	0.2991	0.002

In these expressions $m = \rho A\ell/2$ is the effective mass of the cable, θ is the angle between the cable chord and the horizontal plane, σ_s is the static stress, λ^2 is Irvine's parameter, A is the cross sectional area, ρ is the density, g is the gravitational constant, E is Young's modulus, E_q is the equivalent modulus of the cable, γ is the distributed weight perpendicular to the cable chord, and ω_n is the n-th out-of-plane natural frequency of the cable.

It has been shown with numerical simulations that in the range of $\Omega/\omega_2 \in [0.95, 1.05]$ the averaged equations (2.1) provide an excellent approximation to the full Warnitchai equations for the same three modes; see [9]. Moreover, we checked that the inclusion of the first in-plane mode into the model would result in a noticable response of that additional mode only for $\Omega/\omega_2 > 1.04$. Therefore, we are confident that the model is accurate in the domain of $\Omega/\omega_2 \in [0.95, 1.04]$. In the numerical continuation we vary the parameter over the ranges

$$\Delta/L \in [0, 3.5\times10^{-3}], \quad \Omega/\omega_2 \in [0.95, 1.07].$$

While results for $\Omega/\omega_2 > 1.05$ need to be treated with a degree of caution, we still consider the extended range of Ω/ω_2 up to 1.07 in our bifurcation study. The reason is that this allows us to detect steady-state solutions for large Ω/ω_2 that are then continued back to the region of interest $[0.95, 1.04]$ where their validity is not in doubt; such solutions might otherwise be overlooked.

As the lower cable support is excited vertically at a frequency close to ω_2, from linear dynamics we expect the cable response to be a standing wave in the vertical plane with a sinusoidal shape and fixed mid-span point. These dynamics correspond in equations (2.1) to an equilibrium with a contribution from the basic in-plane mode only (i.e., $Y_1 = Y_2 = 0$); we refer to this equilibrium as the Z_2-mode. Due to the nonlinear behaviour of the cable, beyond certain excitation amplitude and frequency boundaries this pure Z_2-response ceases to be a stable. At such boundaries one or both of the ou-of-plane modes will start to contribute to the dynamics of the cable, and this corresponds to the emergence of stable equilibria of (2.1) with non-zero contributions from Y_1 and Y_2. Note, however, that, because it is directly excited, the basic in-plane mode will always contribute to the dynamics (i.e., Z_2 is always non-zero in the presence of excitation).

Our goal is to present a geometric picture of the different possible equilibrium solutions of (2.1) in dependence on the amplitude Δ/L and the frequency Ω/ω_2 of the excitation. Equations (2.1) are a system of six autonomous ODEs and, hence, their solutions and bifurcations can be followed by means of numerical continuation; we use the software package AUTO [3, 4] for this purpose. The task is to perform systematic continuation runs to find an overall consistent bifurcation diagram of the (constant-amplitude) equilibria of (2.1), their stability and bifurcations. The starting point is the trivial equilibrium for $\Delta/L = 0$ (with zero contribution from all modes) for a fixed frequency Ω/ω_2 close to unity; continuation in Δ/L then allows us to follow the branch of the Z_2-mode. This branch is initially stable but loses stability in different types of bifurcations, of which we find fold (or saddle-node) bifurcations, branch point (or pitchfork) bifurcations and Hopf bifurcations [10, 12, 31].

3. Bifurcation analysis of the mode structure. Our starting point is the bifurcation diagram in the $(\Omega/\omega_2, \Delta/L)$-plane of the (pure) Z_2-mode (with zero contributions from Y_1 and Y_2), which was already considered in [9]. It is shown in figure 2 and features a curve F_{Z_2} of fold bifurcations and curves B_1 and B_2 of branch point bifurcations. (Mathematically, the latter bifurcations are pitchfork bifurcations; the two bifurcating branches of equilibria differ only in the

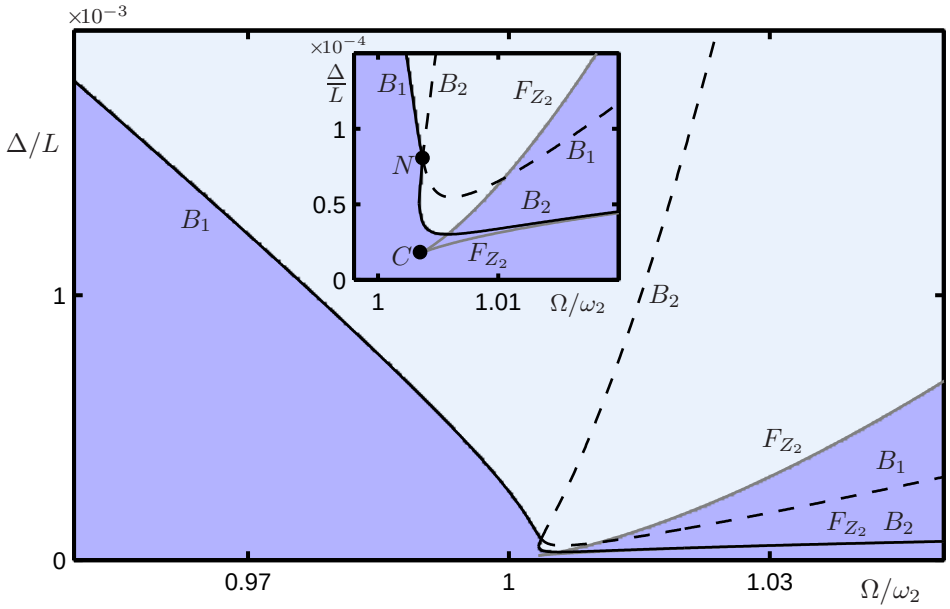

FIG. 2. *Bifurcation diagram in the* $(\Omega/\omega_2, \Delta/L)$*-plane of the* Z_2*-mode of* (2.1)*, showing a curve* F_{Z_2} *of fold bifurcations and curves* B_1 *and* B_2 *of branch point bifurcations. Along solid parts of the curves the bifurcation concerns a stable solution and along dashed parts it concerns an unstable one; the region where the* Z_2*-mode is stable is shaded dark blue. The inset shows an enlargement near* $\Omega/\omega_2 = 1$*.*

phase relationship between the contributing basic modes, which physically corresponds to clockwise or counter-clockwise whirling motion of the cable. Since it is common in the field to represent the coupled modes in terms of their norm $||N||$, these two branches of equilibria are not distinguished; hence, one refers to this bifurcation as a branch point bifurcation.) For any value of Ω/ω_2 the Z_2-mode is stable for sufficiently small Δ/L (dark blue region). Stability of the Z_2-mode is lost when the solid parts of these curves are crossed; such a loss of stability means that Y_1 and/or Y_2 develop a non-zero amplitude. The inset of figure 2, which is an enlargement near $\Omega/\omega_2 = 1$, shows that there is a cusp bifurcation point C on the fold curve F_{Z_2}; moreover, the two curves B_1 and B_2 of branch point bifurcations interact at point N where they exchange their roles as stability boundary for the Z_2-mode.

Figure 2 shows that, when Δ/L is increased the Z_2-mode loses stability in different ways depending on the value of Ω/ω_2. For fixed $\Omega/\omega_2 < 1.003$, the frequency at which point C is located, the branch point curve B_1 is crossed and Y_1 gradually becomes nonzero. For $\Omega/\omega_2 > 1.003$, the upper part of the fold point curve F_{Z_2} (with Δ/L above the cusp point C) is crossed, which leads to a transition to quite different dynamics, where Z_2, Y_1 and Y_2 all contribute. As the inset of figure 2 shows, the stability region of the Z_2-mode extends (from between the points C and N) as a very thin tongue that is bounded by the curve B_2 and the lower part of the fold curve F_{Z_2} (with Δ/L above the cusp point C). When B_2 is crossed Y_2 gradually becomes nonzero; when the lower part of F_{Z_2} is crossed there is a transition to another stable Z_2-mode (of lower amplitude). Hence, this thin tongue constitutes a region of bistability of the Z_2-mode.

This discussion makes clear that the bifurcation diagram in figure 2 is already quite complicated, even though it only concerns the (pure) Z_2-mode. Moreover, it would be quite impractical to try to add to the $(\Omega/\omega_2, \Delta/L)$-plane all the bifurcation curves that bound stability regions of the other coupled mode responses that the system may support. We therefore adopt the more intuitive and

insightful way of representing the stability properties of all modes of the system by representing them as surfaces in $(\Omega/\omega_2, \Delta/L, ||N||)$-space. Starting from the knowledge of the Z_2-mode, branch switching at bifurcation points allows us to follow branches of equilibria with nonzero amplitudes of Y_1 and/or Y_2. Surfaces of the different types of equilibria are then constructed in $(\Omega/\omega_2, \Delta/L, ||N||)$-space from continuation runs in Δ/L for suitably many fixed choices of Ω/ω_2. The rendering of the surface images in this paper is performed with Matlab. Curves of bifurcations are computed by two-parameter continuations and then also plotted in $(\Omega/\omega_2, \Delta/L, ||N||)$-space, where they lie on corresponding surfaces. We find and consider one by one the following types of equilibria of (2.1), which we refer to as the (coupled) modes of (2.1):

1. the Z_2-mode of pure second in-plane mode response (where $Y_1 = Y_2 = 0$); the surface of the Z_2-mode is denoted $\mathcal{L}$.
2. the (Z_2, Y_1)-mode of coupled response between the second in-plane mode and the first out-of plane mode (where $Y_2 = 0$); the surface of the (Z_2, Y_1)-mode is denoted $\mathcal{L}_1$.
3. the (Z_2, Y_2)-mode of coupled response of the second in-plane mode and the second out-of plane mode (where $Y_1 = 0$); the surface of the (Z_2, Y_2)-mode is denoted $\mathcal{L}_2$.
4. the (Z_2, Y_1, Y_2)-mode of coupled response to which all three basic modes contribute; the surface of the (Z_2, Y_1, Y_2)-mode is denoted $\mathcal{L}_{12}$.

3.1. The surface $\mathcal{L}$ of the Z_2-mode. The surface $\mathcal{L}$ of the Z_2-mode in $(\Omega/\omega_2, \Delta/L, ||N||)$-space is shown in figures 3(a) and 4(a) in two different views; also shown are two sets of cross sections in panels (c) and (d) that show the corresponding bifurcation diagram for different fixed values of Δ/L and Ω/ω_2, respectively. Notice how the suface $\mathcal{L}$ is folded along the curve F_{Z_2}. The dark blue part of $\mathcal{L}$ corresponds to the Z_2-mode being stable; this stability region is a single region that is bounded by F_{Z_2} and the respective parts of the branch bifurcation curves B_1 and B_2. Notice how these bifurcation curves from figure 2 are lifted to the surface $\mathcal{L}$, which now also represents the norm $||N||$ of the Z_2-mode; indeed, the bifurcation diagram in the $(\Omega/\omega_2, \Delta/L)$-plane is obtained by projection along $||N||$.

Figure 3(a) shows a view of the surface $\mathcal{L}$ with two intersection curves for fixed Δ/L on it, for $\Delta/L = 0.3\times10^{-5}$ and $\Delta/L = 7\times10^{-5}$, respectively. These curve represent the corresponding cross sections through $\mathcal{L}$, which are one-parameter bifurcation diagrams of the Z_2-mode as a function of the excitation frequency Ω/ω_2; they are plotted in the $(\Omega/\omega_2, ||N||)$-plane in panels (b) and (c). Figure 3(b) shows that for sufficiently small Δ/L the resonant peak of the pure Z_2-response as what one would expect for a linear system: there is a clear peak near 1, the Z_2-mode is a function of Ω/ω_2, and it is stable throughout. However, as the excitation amplitude Δ/L is increased the Z_2-response becomes nonlinear. Figure 3(c) is for $\Delta/L = 7\times10^{-5}$, that is, for a cross section in between the points C and N; see the inset of figure 2. The resonance peak in figure 3(c) is considerably bent to the right, resulting in an S-shape with two fold points. However, there is practically no bi-stability, because the Z_2-mode loses its stability at a branch point B_2 when Ω/ω_2 is increased. The Z_2-mode actually regains stability at a the second branch point labelled B_2, only to lose its stability immediately at the fold point F_{Z_2} (which is virtually indistinguishable from B_2 in figure 3(c); compare with figure 2).

Figure 4(a) shows the surface $\mathcal{L}$ from a different view point, this time with two intersection curves for fixed excitation frequency Ω/ω_2. Panel (b) shows the intersection of $\mathcal{L}$ for $\Omega/\omega_2 = 0.97$ in the $(\Delta/L, ||N||)$-plane, where the Z_2-mode is a monotonically increasing curve; it is stable for sufficiently small Δ/L and then loses stability at the branch bifurcation point B_1. Figure 4(c) shows the Z_2-mode in the $(\Delta/L, ||N||)$-plane for $\Omega/\omega_2 = 1.03$, which is to the right of the points C and N in figure 2. Because the curve F_{Z_2} is now intersected, the branch of the Z_2-mode now has a characteristic S-shape. Stability is lost at the first (right) fold point along the branch. The branch turns around and effectively remains unstable throughout, exept for a tiny interval of Δ/L values just past the second (left) fold point. When Δ/L is increased from zero excitation in an

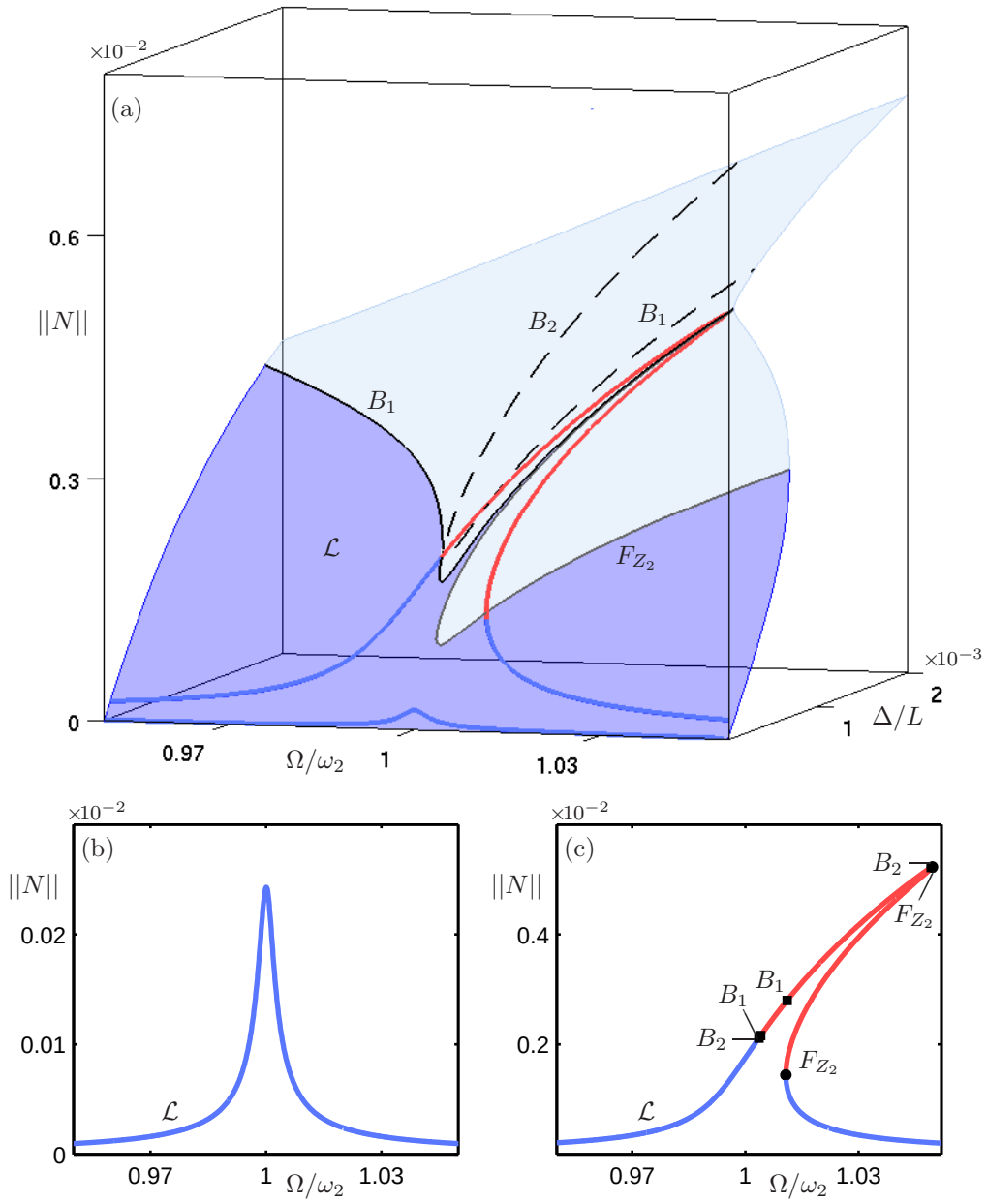

FIG. 3. *Panel (a) shows the surface $\mathcal{L}$ of the Z_2-mode of (2.1) in $(\Omega/\omega_2, \Delta/L, ||N||)$-space. Also shown on $\mathcal{L}$ are the bifurcation curves B_1, B_2 and F_{Z_2} from figure 2; the Z_2-mode is stable in dark blue part and unstable in light blue part. Panels (b) and (c) show the one-parameter bifurcation diagrams in the $(\Omega/\omega_2, ||N||)$-plane for $\Delta/L = 0.3\times10^{-5}$ and for $\Delta/L = 7\times10^{-5}$, respectively; the corresponding curves are highlighted on the surface $\mathcal{L}$. Branch points are denoted by squares and fold points by dots; the Z_2-mode is stable along blue parts of curves and unstable along red parts of curves.*

experiment, one first observes a pure Z_2-response until the fold point is reached and the system

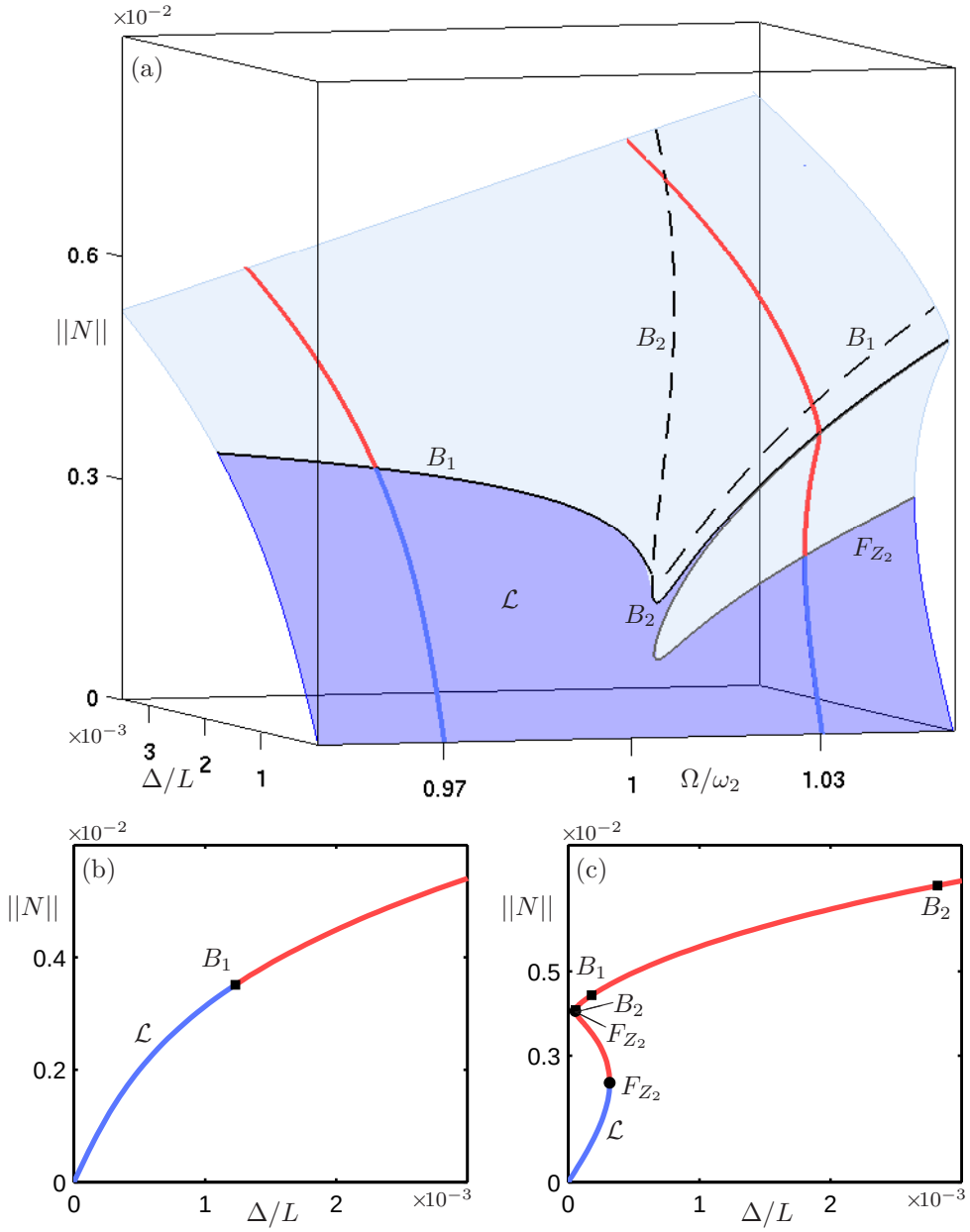

FIG. 4. *Panel (a) shows a different view of the surface $\mathcal{L}$ of the Z_2-mode; compare with figure 3(a). Panels (b) and (c) show the one-parameter bifurcation diagrams in the $(\Delta/L, ||N||)$-plane for $\Omega/\omega_2 = 0.97$ and for $\Omega/\omega_2 = 1.03$, respectively; the corresponding curves are highlighted on the surface $\mathcal{L}$ in panel (a).*

transitions to a different, as yet unknown, solution.

Clearly, to understand the response of the cable for values of Ω/ω_2 where the Z_2-mode is unstable one needs to consider the (surface of) bifurcating equilibria with non-trivial contributions from Y_1 and/or Y_2; they are discussed in the subsequent sections.

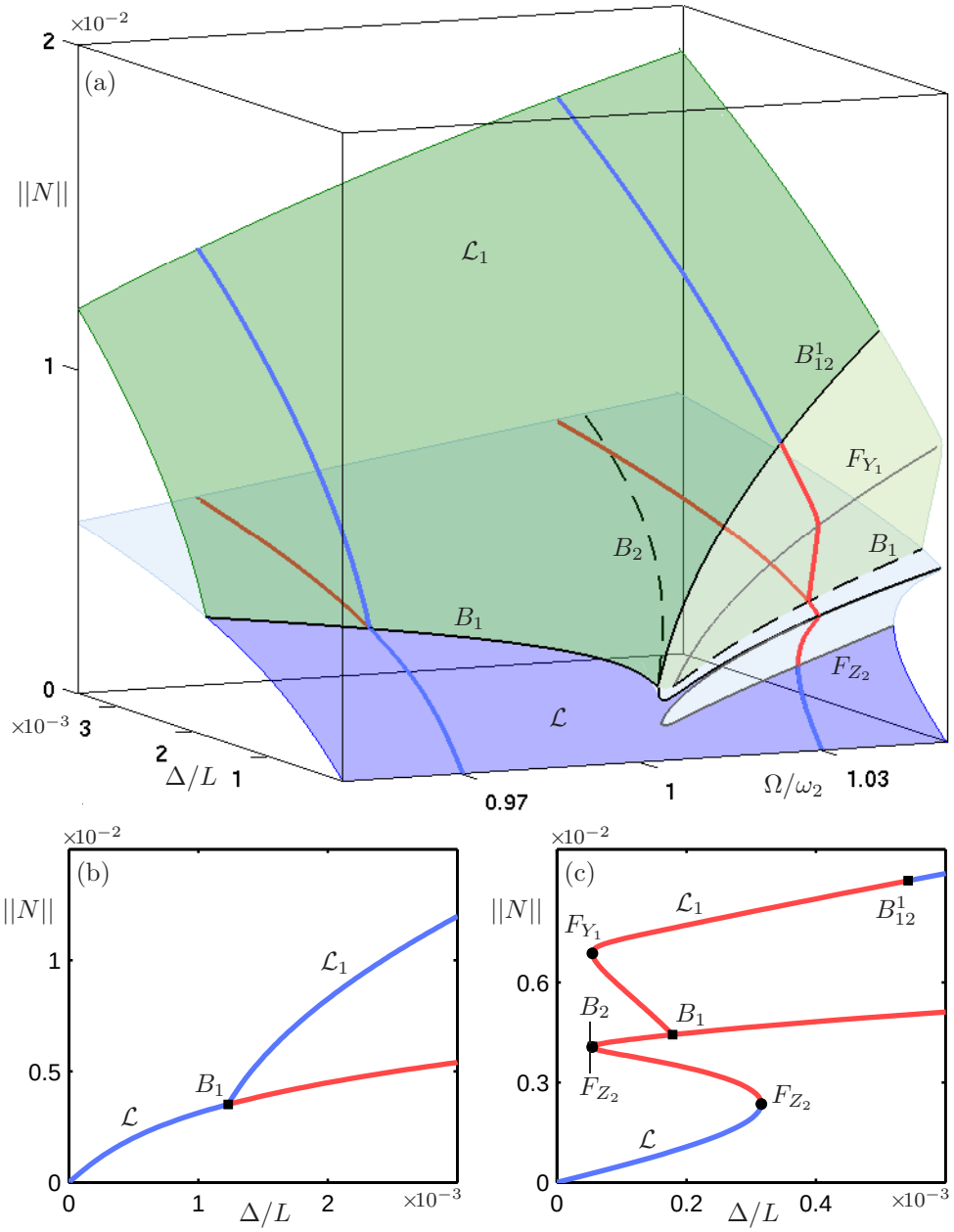

FIG. 5. *Panel (a) shows the surface $\mathcal{L}_1$ (green) of the (Z_2, Y_1)-mode of (2.1) in $(\Omega/\omega_2, \Delta/L, ||N||)$-space, and how it connects to the surface $\mathcal{L}$ (blue) from figure 4. Also shown on $\mathcal{L}_1$ are the bifurcation curves B_{12}^1 and F_{Y_1}; the (Z_2, Y_1)-mode is stable in dark green part and unstable in light green part. Panels (b) and (c) show the one-parameter bifurcation diagrams in the $(\Delta/L, ||N||)$-plane for $\Omega/\omega_2 = 0.97$ and for $\Omega/\omega_2 = 1.03$, respectively; the corresponding curves are highlighted on the surfaces $\mathcal{L}_1$ and $\mathcal{L}$ in panel (a).*

3.2. The surface $\mathcal{L}_1$ of the (Z_2, Y_1)-mode. The (Z_2, Y_1)-mode bifurcates from the Z_2-mode along the branch bifurcation curves B_2. Figure 5(a) shows the associated surface $\mathcal{L}_1$ (green) of the (Z_2, Y_1)-mode in $(\Omega/\omega_2, \Delta/L, ||N||)$-space, which connects to the surface $\mathcal{L}$ (blue) along the curve

B_1. The stable part of $\mathcal{L}_1$ (dark green) is bounded by the curve B_1 on $\mathcal{L}$ and by the branch bifurcation curve B^1_{12} on $\mathcal{L}_1$; as we will see in section 3.4, the surface $\mathcal{L}_{12}$ of the (Z_2, Y_1, Y_2)-mode connects along B^1_{12}. Notice also the fold along F_{Y_1}. Highlighted in figure 5(a) are the cross sections of $\mathcal{L}$ and $\mathcal{L}_1$ for $\Omega/\omega_2 = 0.97$ and $\Omega/\omega_2 = 1.03$. Figure 5(b) shows the corresponding bifurcation diagram for $\Omega/\omega_2 = 0.97$ in the $(\Delta/L, ||N||)$-plane, which shows that a stable branch of the (Z_2, Y_1)-mode bifurcates from the Z_2-mode at the point B_1; compare with figure 4(b). The corresponding bifurcation diagram for $\Omega/\omega_2 = 1.03$ in the $(\Delta/L, ||N||)$-plane is shown in figure 5(c). An unstable branch of (Z_2, Y_1)-mode bifurcates from the point B_1, where the Z_2-mode itself is also unstable. The branch of the (Z_2, Y_1)-mode remains unstable after the fold point F_{Y_1} but becomes stable after the branch point B^1_{12}. Overall, figure 5 shows that, for any value of Ω/ω_2 the (Z_2, Y_1)-mode may be observed stably provided the excitation ampitude Δ/L is sufficiently large.

As it turns out, there is an additional part of the (Z_2, Y_1)-mode surface $\mathcal{L}_1$ that can be found when one considers it over a larger range of Ω/ω_2-values. Figure 6(a) shows the two surfaces $\mathcal{L}_1$ and $\mathcal{L}$ for $\Omega/\omega_2 \in [1.0, 1.07]$. Because of its complicated shape, the new part of the surface $\mathcal{L}_1$ is not rendered as a surface but represented by equally spaced (green) intersection curves for fixed Ω/ω_2. These intersection curves are connected for fixed $\Omega/\omega_2 > 1.05$ to the main part of the surface $\mathcal{L}_1$ at two fold curves, which connect to the fold curve F_{Y_1} at $\Omega/\omega_2 \approx 1.05$. However, for fixed $\Omega/\omega_2 < 1.05$ we find figure-of-eight shaped isolas. Panels (b) and (c) of figure 6 show the two slices for $\Omega/\omega_2 = 1.03$ and for $\Omega/\omega_2 = 1.06$, respectively, which are also highlighted in panel (a). Notice the new isola of the (Z_2, Y_1)-mode for $\Omega/\omega_2 = 1.03$ in figure 6(b) compared with figure 5(c). In the section for $\Omega/\omega_2 = 1.06$, on the other hand, we find a single connected curve of the (Z_2, Y_1)-mode. In both cases, there is a small region of stable (Z_2, Y_1)-response on the new curve.

Since these features of the surface $\mathcal{L}_1$ are hard to see on the scale of figure 6, we now focus on how the isola in the $(\Delta/L, ||N||)$-plane connects to the remainder of $\mathcal{L}_1$ as Ω/ω_2 is increased through 1.05. Figure 7 shows the intersection curves of $\mathcal{L}_1$ with cross sections for $\Omega/\omega_2 = 1.04$, for $\Omega/\omega_2 = 1.05$ and for $\Omega/\omega_2 = 1.06$ in the relevant part of the $(\Delta/L, ||N||)$-plane. Notice the figure-eight shape of the isola for $\Omega/\omega_2 = 1.04$ in figure 7(a); it is not actually connected at the two intersection point with the other intersection curve of $\mathcal{L}_1$. There are four fold points on the isola, which are labelled F_{Y_1} and F''_{Y_1}. At the moment of transition at $\Omega/\omega_2 \approx 1.05$ the lower fold point F_{Y_1} on the isola coincides with the fold point F_{Y_1} on the other branch; see figure 7(b). For $\Omega/\omega_2 = 1.06$ as in figure 7(c), there is now a single connected intersection curve of $\mathcal{L}_1$; the degenerate fold point has split up into two fold points labelled F'_{Y_1}. Notice that close to these fold points there are two branch points that are labelled B^1_{12}; as we will see in section 3.4, they lead to the bifurcating (Z_2, Y_1, Y_2)-mode.

Overall, figure 7 shows that the connectivity of the local branches near the point of transition changes. This corresponds to a transition of the cross section through a critical point on the surface $\mathcal{L}_1$ in $(\Omega/\omega_2, \Delta/L, ||N||)$-space. The two fold curves F_{Y_1} and F'_{Y_1} on $\mathcal{L}_1$ have a maximum and a minimum with respect to Ω/ω, respectively, and intersect transversally at this special point. The curve F'_{Y_1} with its minimum can be seen in figure 6(a). Of the curve F_{Y_1} only the part up to the maximum where it meets F'_{Y_1} is shown; its other part lies on the isola (green loops) and it is not shown in figure 6(a). Note that the curve of branch point bifurcations B_{12} also passes through the critical point on $\mathcal{L}_1$ and has a minimum there with respect to Ω/ω. The isola can be found in the cross section for fixed Ω/ω_2 in the range $\Omega/\omega_2 \in (1.02, 1.05)$; see figure 6(a). It disappears at $\Omega/\omega_2 \approx 1.02$ by shrinking down to a point, which corresponds to a minimum with respect to Ω/ω_2 of the curve F_{Y_1} in $(\Omega/\omega_2, \Delta/L, ||N||)$-space.

In all three panels of figure 7 we also find a pair of Hopf bifurcations (denoted by asterisks). Moreover, the (Z_2, Y_1)-mode on the new part of $\mathcal{L}_1$ is stable between the (upper) fold point F_{Y_1} and the left-most point of Hopf bifurcation. Hence, we have found a new observable (Z_2, Y_1)-response of the cable in the region of interest $\Omega/\omega_2 \in [0.95, 1.04]$, which is not connected to the main part

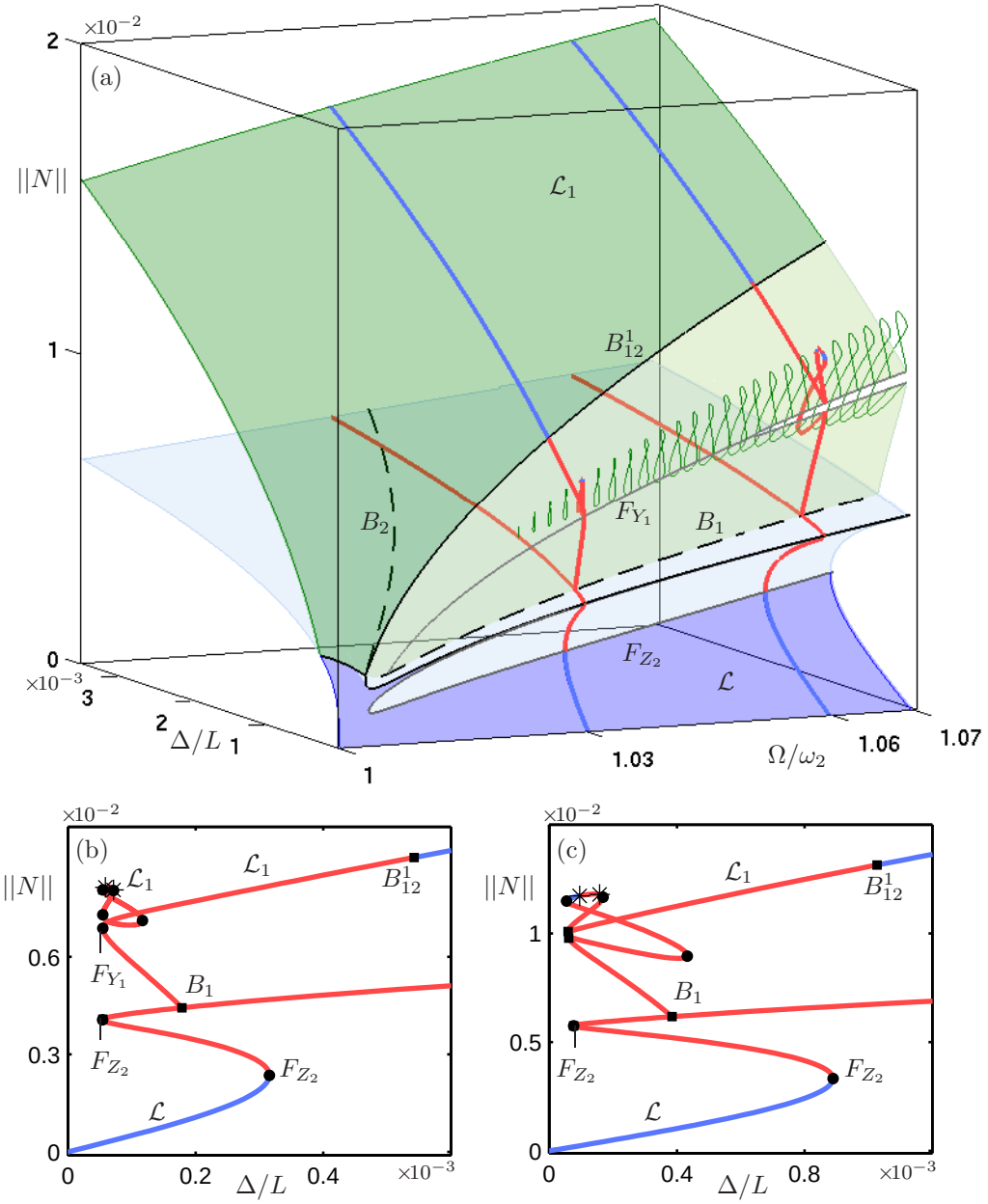

FIG. 6. *Panel (s) shows the surfaces $\mathcal{L}_1$ (green) and $\mathcal{L}$ (blue) in $(\Omega/\omega_2, \Delta/L, ||N||)$-space over the range $\Omega/\omega_2 \in [1.0, 1.07]$. The new feature is an additional part of the surface $\mathcal{L}_1$ that is connected to its main part for $\Omega/\omega_2 > 1.05$ along two fold curves, but also extends to smaller values of Ω/ω_2; due to its complicated shape, this new part of $\mathcal{L}_1$ is represented by intersections curves for fixed Ω/ω_2. The respective intersections for $\Omega/\omega_2 = 1.03$ and for $\Omega/\omega_2 = 1.06$ are highlighted. The corresponding bifurcation diagrams in the $(\Delta/L, ||N||)$-plane are shown in panels (b) and (c); there are two points of Hopf bifurcation (indicated by asterisks) on the additonal branches of the (Z_2, Y_1)-mode.*

of the surface $\mathcal{L}_1$ in this range of Ω/ω_2. This discovery justifies the consideration of the extended

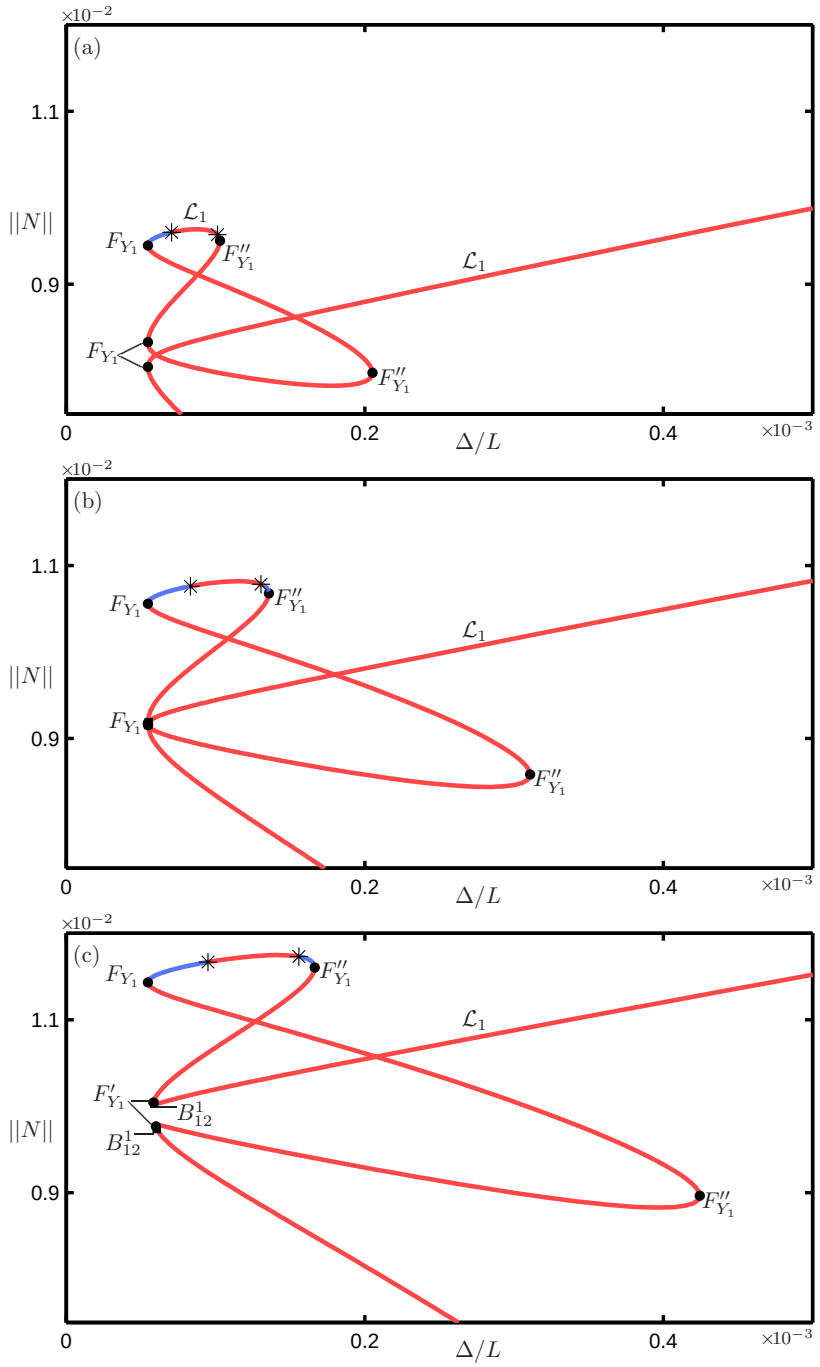

FIG. 7. *One-parameter bifurcation diagrams of the (Z_2, Y_1)-mode in the $(\Delta/L, ||N||)$-plane for $\Omega/\omega_2 = 1.04$ in panel (a), for $\Omega/\omega_2 = 1.05$ in panel (b), and for $\Omega/\omega_2 = 1.06$ in panel (c). The ranges of Δ/L and $||N||$ are chosen to show how the isola of the (Z_2, Y_1)-mode for $\Omega/\omega_2 < 1.05$ connects to the remainder of the surface $\mathcal{L}_1$ when Ω/ω_2 is increased through $\Omega/\omega_2 \approx 1.05$; compare with figure 6.*

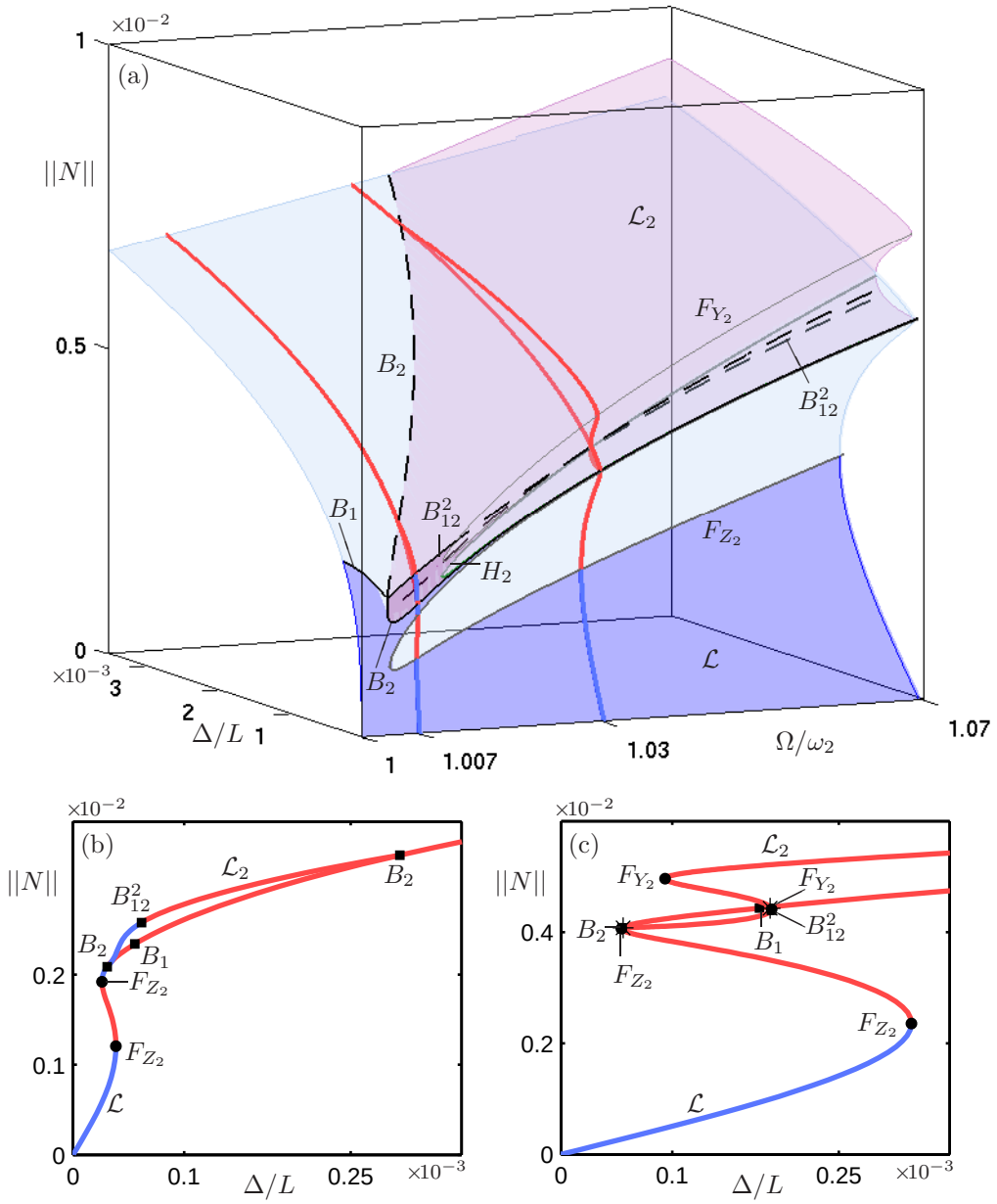

FIG. 8. *Panel (a) shows the surface $\mathcal{L}_2$ (purple) of the (Z_2, Y_2)-mode of (2.1) in $(\Omega/\omega_2, \Delta/L, ||N||)$-space, and how it connects to the surface $\mathcal{L}$ (blue) from figure 4. Also shown on $\mathcal{L}_2$ are the bifurcation curves F_{Y_2} and B_{12}^1; the (Z_2, Y_2)-mode is stable in the small dark purple part only. Panels (b) and (c) show the one-parameter bifurcation diagrams in the $(\Delta/L, ||N||)$-plane for $\Omega/\omega_2 = 1.007$ and for $\Omega/\omega_2 = 1.03$, respectively; the corresponding curves are highlighted on the surfaces $\mathcal{L}_2$ and $\mathcal{L}$ in panel (a).*

range of Ω/ω_2.

3.3. The surface $\mathcal{L}_2$ of the (Z_2, Y_2)-mode. Figure 8(a) shows the surface $\mathcal{L}_2$ of the (Z_2, Y_2)-mode, which is attached to the surface $\mathcal{L}$ along the branch bifurcation curve B_2. Almost all of $\mathcal{L}_2$

is unstable (light purple), but there is a small stable region (dark purple) near $\Omega/\omega_2 = 1$. On $\mathcal{L}_2$ there is a curve F_{Z_2} of fold bifurcation, whose left-most point is a cusp point. Moreover, we find a curve B^2_{12} of branch point bifurcation that emerges from the point N where B_1 and B_2 intersect on $\mathcal{L}$; see figure 2. As with previous plots, two intersection sets are highlighted, namely those for $\Omega/\omega_2 = 1.007$ and $\Omega/\omega_2 = 1.03$, respectively; they are shown in the $(\Delta/L, ||N||)$-plane panels (b) and (c) of figure 8.

The section for $\Omega/\omega_2 = 1.007$ in figure 8(b) passes through the stable part of $\mathcal{L}_2$. The branch $\mathcal{L}_2$ of the (Z_2, Y_2)-mode connects to the branch $\mathcal{L}$ of the Z_2-mode at the two branch bifurcation points labelled B_2. The (Z_2, Y_2)-mode is stable right after the left-most branch bifurcation point B_2 on $\mathcal{L}$, and it loses its stability at the branch point B^2_{12}; as we will see in 3.4, the (Z_2, Y_1, Y_2)-mode can be observed stably past this point. Notice from figure 8(b) that, as the excitation amplitude Δ/L is increased from zero, one first observes the Z_2-mode until the fold point F_{Z_2} is reached, where the system transitions to a stable (Z_2, Y_2)-response.

The section for $\Omega/\omega_2 = 1.03$ in figure 8(c), on the other hand, misses the stable part on $\mathcal{L}_2$. Consequently, the branch $\mathcal{L}_2$ bifurcating from B_2 is unstable throughout, until it also reconnects with the branch of the Z_2-mode at a second branch bifurcation point B_2 (which is outside the Δ/L-range shown in figure 8(c)). Notice the S-shaped nature of the branch $\mathcal{L}_2$ with two fold curves labelled F_{Z_2}.

3.4. The surface $\mathcal{L}_{12}$ of the (Z_2, Y_1, Y_2)-mode. The surface $\mathcal{L}_{12}$ of the (Z_2, Y_1, Y_2)-mode is quite complicated because it connects the two surfaces $\mathcal{L}_1$ of the (Z_2, Y_1)-mode and $\mathcal{L}_2$ of the (Z_2, Y_2)-mode. In figure 9(a), it is shown together with only the surface $\mathcal{L}_2$ from figure 8(a) to which it is attached along the curve B^2_{12}. The (dark brown) stable part of $\mathcal{L}_{12}$ in figure 9(a) is bounded at the top by the curve B^1_{12}, along which this surface is connected to the surface $\mathcal{L}_1$ of the (Z_2, Y_1)-mode (which is not shown); compare with figure 6(a). The lower boundary of the stable part of $\mathcal{L}_{12}$ is more complicated: at low values of Ω/ω_2 it is the same curve B^2_{12}, and for higher values of Ω/ω_2 it is formed by fold curve $F_{Y_{12}}$ on $\mathcal{L}_{12}$. Specifically, between $F_{Y_{12}}$ and B^2_{12} there are two other boundaries of $\mathcal{L}_{12}$, namely the fold curve $F^1_{Y_{12}}$ and the Hopf bifurcation curve H_2. In fact, $F^1_{Y_{12}}$ emerges from a point on B^2_{12} and H_2 emerges from a point on B^2_{12}. This structure of the boundary of the (Z_2, Y_1)-mode was also found in [15] for a four-mode model that includes the first in-plane mode.

Two of the three highlighted intersection sets in figure 9(a) are shown separately in the $(\Delta/L, ||N||)$-plane as panels (b) and (c); for clarity, the stable and unstable regions of $\mathcal{L}$ are also shown as black and grey curves, respectively. In figure 9(b) for $\Omega/\omega_2 = 1.007$, which builds on figure 8(b), the branch $\mathcal{L}_{12}$ bifurcates from the point B^2_{12} on the branch $\mathcal{L}_2$; along this branch the (Z_2, Y_1, Y_2)-mode is stable. Figure 9(c) for $\Omega/\omega_2 = 1.03$ builds on figure 8(c). Now the branch $\mathcal{L}_{12}$ has three fold points; it is stable only after the last fold point labelled $F_{Y_{12}}$. Notice that in between the upper fold point and a point H_{12} of Hopf bifurcation (denoted by an asterisk) there is an additional tiny part of the branch where the (Z_2, Y_1, Y_2)-mode is stable; this Hopf bifurcation curve is shown in figure 9(a). Finally, we remark that figure 9(c) shows that, as Δ/L is increased from zero, the transition to different dynamics when the Z_2-mode loses stability at F_{Z_2} now results in a (Z_2, Y_1, Y_2)-response of the cable.

3.5. The bifurcation diagram consiting of all mode surfaces. Figure 10 shows the surfaces $\mathcal{L}$ (blue), $\mathcal{L}_1$ (green), $\mathcal{L}_2$ (purple) and $\mathcal{L}_{12}$ (brown) together in $(\Omega/\omega_2, \Delta/L, ||N||)$-space. It constitutes a bifurcation diagram of the Z_2-mode, the (Z_2, Y_1)-mode, the (Z_2, Y_2)-mode and the (Z_2, Y_1, Y_2)-mode, which represent all the steady-state solutions of (2.1) and, hence, the responses of the cable with fixed amplitudes of the contributing three basic in-plane and out-of-plane modes. These different surfaces meet at curves of branch point bifurcations; specifically, $\mathcal{L}_1$ meets $\mathcal{L}$ along B_1 (see section 3.2 and figure 6), $\mathcal{L}_2$ meets $\mathcal{L}$ along B_2 (see section 3.3 and figure 8), and $\mathcal{L}_{12}$ meets $\mathcal{L}_1$ along B^1_{12} and $\mathcal{L}_2$ along B^2_{12} (see section 3.4, and figure 9). Stable parts of the surfaces are

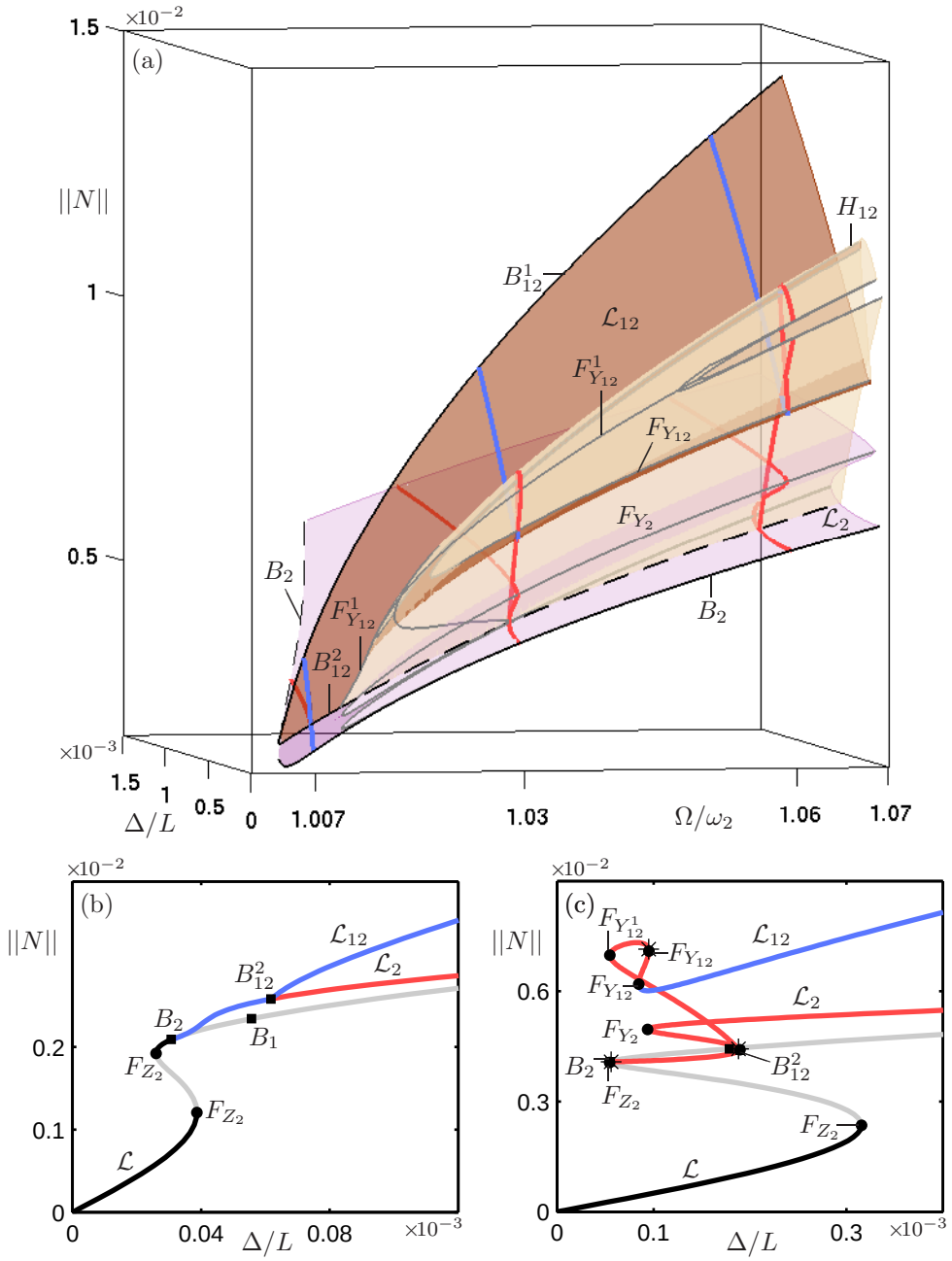

FIG. 9. *Panel (a) shows the surface $\mathcal{L}_{12}$ (brown) of the (Z_2, Y_1, Y_2)-mode of (2.1) in $(\Omega/\omega_2, \Delta/L, ||N||)$-space, and how it connects to the surface $\mathcal{L}_2$ (purple) from figure 8. Also shown on $\mathcal{L}_2$ is the fold curve $F_{Y_{12}}$; the (Z_2, Y_1, Y_2)-mode is stable in the dark brown part of $\mathcal{L}_{12}$ and unstable in the light brown part. The intersection sets for $\Omega/\omega_2 = 1.007$, for $\Omega/\omega_2 = 1.03$, and for $\Omega/\omega_2 = 1.06$ are highlighted; those for $\Omega/\omega_2 = 1.007$ and for $\Omega/\omega_2 = 1.03$ are shown in the $(\Delta/L, ||N||)$-plane, and that for $\Omega/\omega_2 = 1.007$ appears as part of figure 11(c).*

represented by darker colours and unstable parts by lighter colours; the respective curves of branch point bifurcations are shown as solid curves where they connect two stable surfaces and as dashed

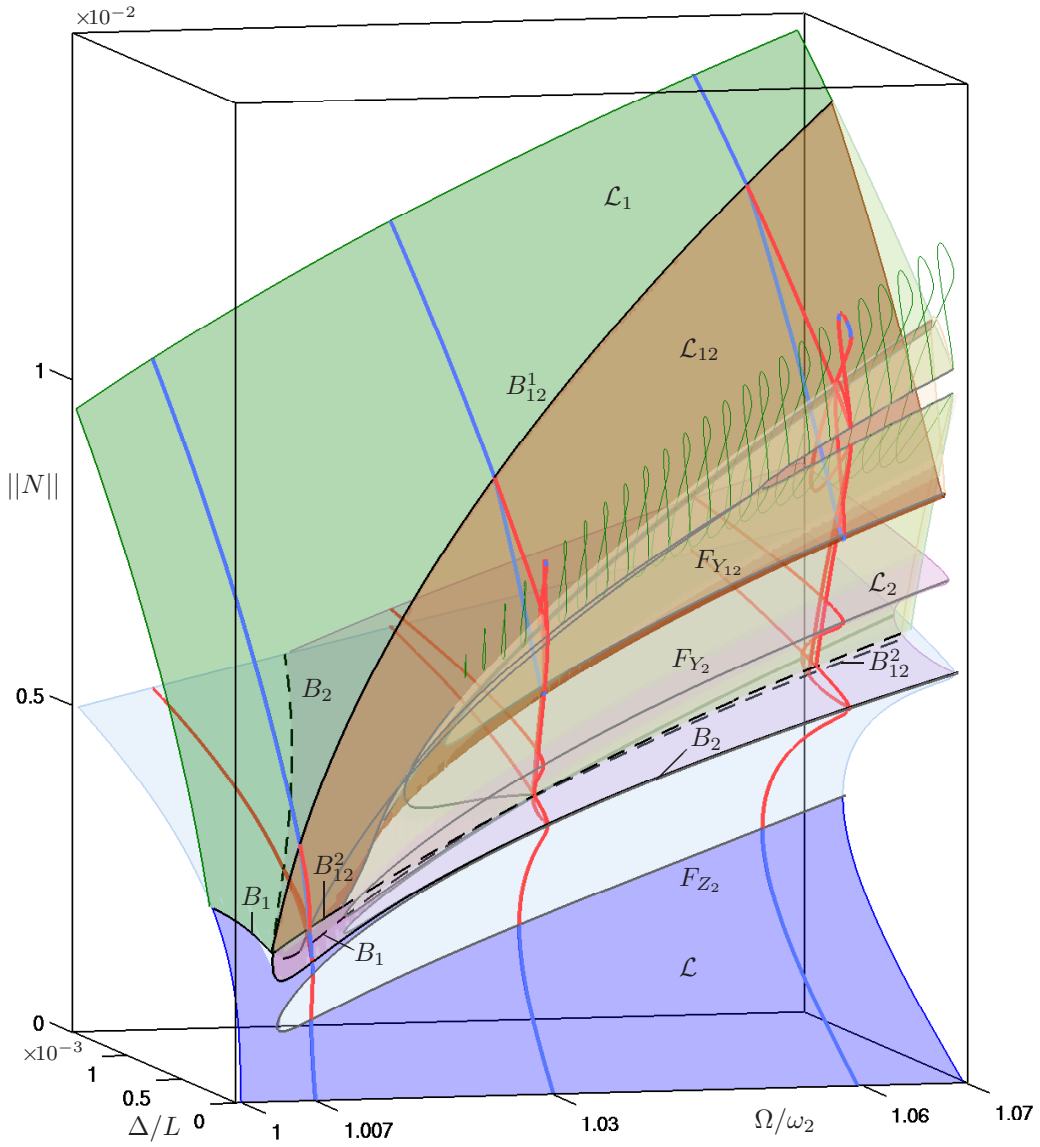

FIG. 10. *The surfaces $\mathcal{L}$ (blue), $\mathcal{L}_1$ (green), $\mathcal{L}_2$ (purple) and $\mathcal{L}_{12}$ (brown) shown together in $(\Omega/\omega_2, \Delta/L, ||N||)$-space together with the various curves of bifurcations on them. The intersection sets for $\Omega/\omega_2 = 1.007$, $\Omega/\omega_2 = 1.03$ and $\Omega/\omega_2 = 1.06$ are highlighted; darker colours represent stable modes.*

curves where they connect two unstable surfaces. Also shown in figure 10 are the different curves of fold bifurcation.

The bifurcation diagram in figure 10 is shown for the range $\Omega/\omega_2 \in [1.0, 1.07]$ where the surfaces and corresponding modes interact strongly. Note that for $\Omega/\omega_2 \leq 1$, only the surfaces $\mathcal{L}$ and $\mathcal{L}_1$ meet along the curve B_1; see figures 5 and 6. This is visible already on the left-hand side of figure 10, so that this bifurcation diagram represents the topological nature of the equilibria of (2.1) and their stability over the entire range of $\Omega/\omega_2 \in [0.97, 1.0]$ that we consider here. As before,

even though it may be at the limit of validity of the three-mode model (2.1) considered here, the range $\Omega/\omega_2 \in [1.04, 1.07]$ is specifically included due to the nature of the surface $\mathcal{L}_1$.

The three intersection sets for $\Omega/\omega_2 = 1.007$, $\Omega/\omega_2 = 1.03$ and $\Omega/\omega_2 = 1.06$ are highlighted on the surfaces in figure 10. They are shown as one-parameter bifurcation diagrams for all of the modes in the $(\Delta/L, ||N||)$-plane in 11(a)–(c).

For fixed $\Omega/\omega_2 = 1.007$ in figure 11(a), as Δ/L is increased from zero, the cable first experiences vibrations in the Z_2-mode. At F_{Z_2} a transition occurs to the stable part of the branch $\mathcal{L}_2$ of the (Z_2, Y_2)-mode, meaning that now the second out-of-plane mode also contributes to the cable response. When Δ/L is increased further, past B^2_{12}, one observes also the gradual onset of the first out-of-plane mode to the cable response when B^2_{12} is crossed to the stable part of the branch $\mathcal{L}_{12}$. For even higher Δ/L the contribution from Y_2 disappears gradually at B^1_{12}, and one is left with the (Z_2, Y_1)-mode along the stable part of $\mathcal{L}_1$. When Δ/L is decreased again, one observes a gradual transition from the (Z_2, Y_1)-mode via the (Z_2, Y_1, Y_2)-mode and the (Z_2, Y_2)-mode to the Z_2-mode. However, there is then a transition at F_{Z_2} to the lower branch of $\mathcal{L}$, that is, to a Z_2-mode with lower amplitude, which is part of a small hysteresis loop.

For fixed $\Omega/\omega_2 = 1.03$ in figure 11(b) the bifurcation diagram in the $(\Delta/L, ||N||)$-plane is considerably more complicated. The transition from the stable Z_2-mode at F_{Z_2} now results in a (Z_2, Y_1, Y_2)-mode response of the cable along the stable part of $\mathcal{L}_{12}$. When Δ/L is increased the Y_2-contribution gradually disappears at B^1_{12}, and one is again left with the (Z_2, Y_1)-mode along the stable part of $\mathcal{L}_1$. When Δ/L is decreased, starting from the stable part of $\mathcal{L}_{12}$, the (Z_2, Y_1, Y_2)-mode response is observed until the fold point $F_{Z_{12}}$ is reached. Then the system transtions to different dynamics. It is actually not entirely clear from the bifurcation diagram in figure 11(b) to which repsonse the system will move at this point. After all, there is now a considerable amount of multi-stability between different modes. Moreover, there are points of Hopf bifurcation (denoted by asterisks) that give rise to periodic solutions, some of which are stable, for example, past the left-most Hopf bifurcation on the isola of $\mathcal{L}_1$. There is also the possibility that such periodic orbits bifurcate further to more complicated stable dynamics of the cable. The bifurcation study of periodic solutions and their bifurcations is beyond the study presented here and will be reported elsewhere.

Finally, for $\Omega/\omega_2 = 1.06$ in figure 11(c) the one-parameter bifurcation diagram is very much as that for $\Omega/\omega_2 = 1.03$ in figure 11(b). As was discussed in section 3.2, the difference is that $\mathcal{L}_1$ is a single branch that now incorporates the former isola. However, in terms of observed stable behaviour of the cable, the two cases are effectively the same.

From a practical point of view, it is useful to be able to identify for which combination of excitation frequency and amplitude the different types of coupled mode response of the cable can be found. Therefore, we present in figure 12(a) a projection of the stable parts of the surfaces $\mathcal{L}_1$ (green), $\mathcal{L}_2$ (purple) and $\mathcal{L}_{12}$ (brown) onto the relevant part of the $(\Omega/\omega_2, \Delta/L)$-plane. For comparison, the stability region of the Z_2-mode, corresponding to the stable part of the surface $\mathcal{L}$, is shown in blue in figure 12(b). Note that the Z_2-mode is stable throughout the white region in figure 12(a); moreover, to the right of the point N the stability regions in panels (a) and (b) of figure 12 overlap, yielding a considerable region of multistability between different cable responses. Overall, figure 12 represents a practical bifurcation chart for the observable mode dynamics of the cable.

In figure 12(a) we show only the bifurcation curves that bound the respective stability regions. They include the curves $H_2 \in \mathcal{L}_2$ and $H_{12} \in \mathcal{L}_{12}$ of Hopf bifurcations, which bound the stability regions of $\mathcal{L}_2$ and $\mathcal{L}_{12}$, respectively. Notice, in particular, the very thin strip of the (purple) stability region of $\mathcal{L}_2$ that is bounded by the curves B_2 and H_2. Similarly, there is an extremely thin strip of the stability region of $\mathcal{L}_{12}$ between the curves $F_{Y_{12}}$ and H_{12}, which correspond to a region of bi-stability of the (Z_2, Y_1, Y_2)-mode. We remark that these two thin strips of stability would be

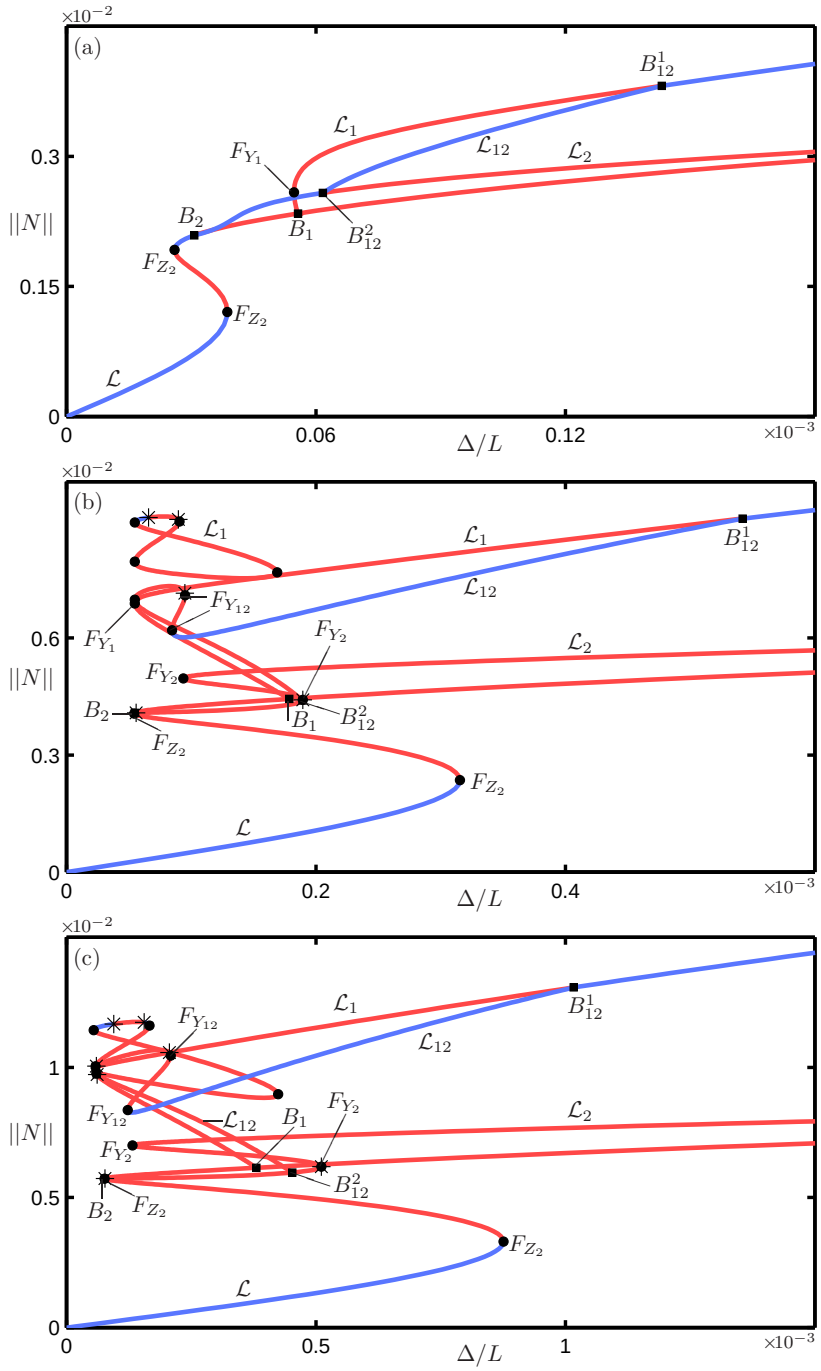

FIG. 11. *One-parameter bifurcation diagrams in the* $(\Delta/L, ||N||)$*-plane for* $\Omega/\omega_2 = 1.007$ *in panel (a), for* $\Omega/\omega_2 = 1.03$ *in panel (b), and for* $\Omega/\omega_2 = 1.06$ *in panel (c). Blue curves denote stable and red curves denote unstable solutions, branch points are denoted by squares, fold points by dots, and Hopf bifurcation points by asterisks.*

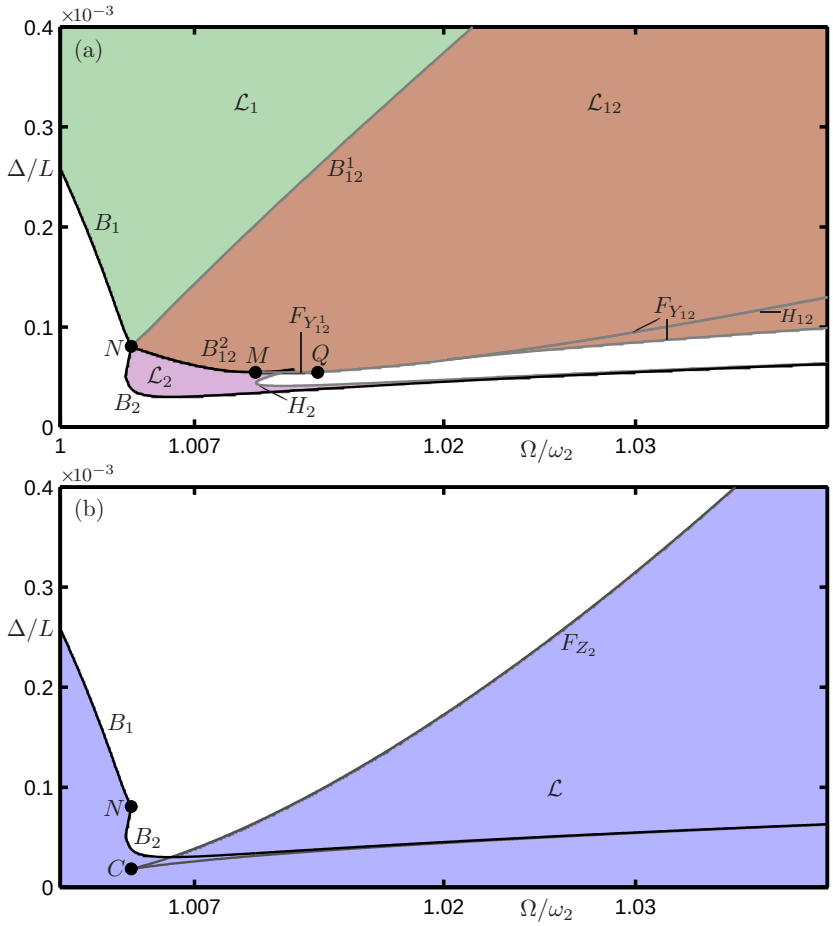

FIG. 12. *Panel (a) shows the projection of the stable parts of the surfaces $\mathcal{L}_1$ (green), $\mathcal{L}_2$ (purple) and $\mathcal{L}_{12}$ (brown) onto the $(\Omega/\omega_2, \Delta/L)$-plane, where $\Omega/\omega_2 \in [1, 1.04]$ and $\Delta/L \in [0, 0.0075]$. Panel (b) shows the stable part of the surface $\mathcal{L}$ in the same region of the $(\Omega/\omega_2, \Delta/L)$-plane.*

virtually impossible to find in an experiment. However, if another parameter, such as the damping ratio, is changed then these regions of bistability may be considerably bigger [29].

3.6. Frequency responce of the cable. Most one-parameter bifurcation diagrams we presented are in terms of changing excitation amplitude Δ/L for a specific fixed value of the excitation frequency Ω/ω_2. In fact, the entire bifurcation diagram in figure 10 has been built up by the corresponding sections for a set of fixed values of Ω/ω_2, because this choice facilitates the rendering of the different surfaces involved. It is quite common, on the other hand, to characterize a periodically driven system experimentally by its frequency response, that is, by performing a sweep in the excitation frequency for a given fixed value of the excitation amplitude. Indeed, such one-parameter continuations in Ω/ω_2 can be obtained from the bifurcation diagram in figure 10 as cross sections for fixed Δ/L. We now discuss their properties in more detail.

The starting point of our investigation is the nonlinear response of the Z_2-mode in figure 3(c), where the Z_2-mode is actually mostly unstable around the resonance peak of the frequency response for $\Delta/L = 7 \times 10^{-5}$. We are now in a position to consider what other modes are observed, and

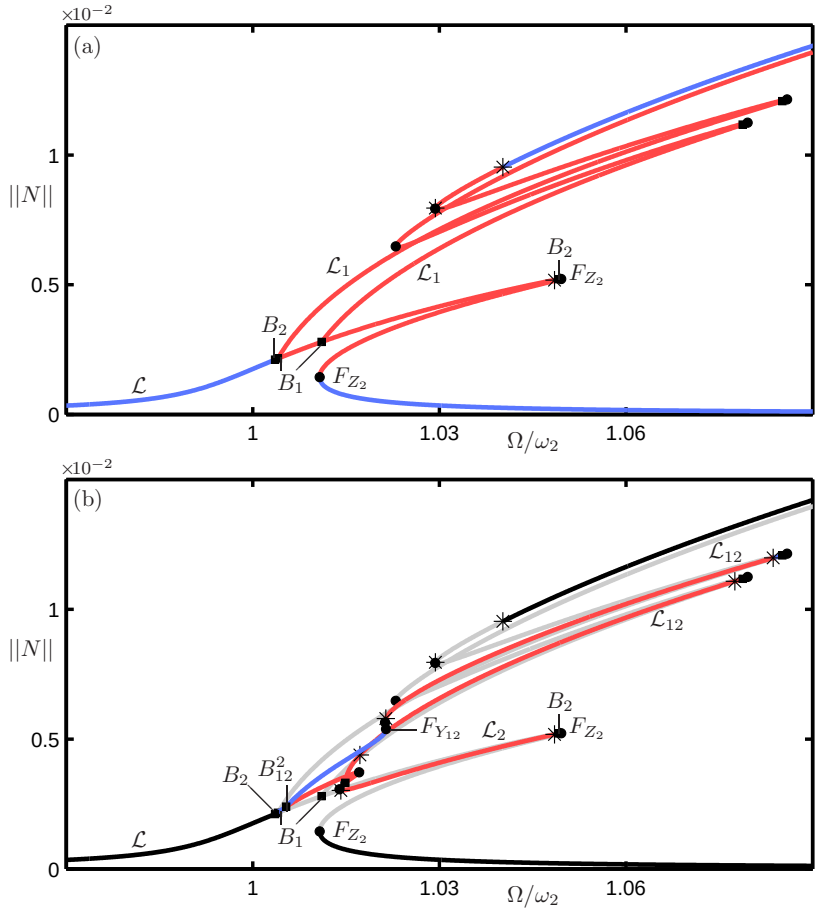

FIG. 13. *One-parameter bifurcation diagram in the* $(\Omega/\omega_2, ||N||)$*-plane for* $\Delta/L = 7 \times 10^{-5}$*. Panel (a) shows only the branches* $\mathcal{L}$ *and* $\mathcal{L}_1$*, and in panel (b) the branches* $\mathcal{L}_2$ *and* $\mathcal{L}_{12}$ *(coloured) are added to* $\mathcal{L}$ *and* $\mathcal{L}_1$ *(black and grey).*

the result is shown in figure 13 over an extended range of Ω/ω_2. Panel (a) repeats the branch $\mathcal{L}$ of the Z_2-mode and also shows the bifurcating branch $\mathcal{L}_1$ of the (Z_2, Y_1)-mode. The branch $\mathcal{L}_1$ is quite a complicated curve with a large number of fold points. Figure 13(b) repeats the branches $\mathcal{L}$ and $\mathcal{L}_1$ (in black and grey) and also shows the branches $\mathcal{L}_2$ and $\mathcal{L}_{12}$. The overall picture of frequency response is quite complicated; this is a manifestation of the considerable nonlinearity in the coupling between the basic in-plane and the two out-of-plane modes. At low frequencies the cable response is purely in the Z_2-mode. As Ω/ω_2 increases past the branch point B_2 a change to the coupled (Z_2, Y_2)-mode is observed. At a slightly higher frequency of $\Omega/\omega_2 \approx 1.005$ the point B_{12}^2 is passed and there is a gradual transitions to a coupled (Z_2, Y_1, Y_2)-mode response. The stable part of the branch $\mathcal{L}_{12}$ ends at $F_{Y_{12}}$, which suggest that the cable response transitions down to the pure Z_2-mode. Notice the hysteresis loop due to the transition up to the (Z_2, Y_1, Y_2)-mode at the point F_{Y_2} when Ω/ω_2 is decreased again.

Figure 14 shows the frequency response for $\Delta/L = 6.3 \times 10^{-4}$, where again panel (a) only shows $\mathcal{L}$ and $\mathcal{L}_1$, and panel (c) adds $\mathcal{L}_2$ and $\mathcal{L}_{12}$. Notice that there is now a larger range of Ω/ω_2 where the (Z_2, Y_1)-mode is stable before the (Z_2, Y_1, Y_2)-mode is observed for larger values of Ω/ω_2. Moreover, the (Z_2, Y_1, Y_2)-mode is then stable throughout the entire large range of Ω/ω_2 in figure 14.

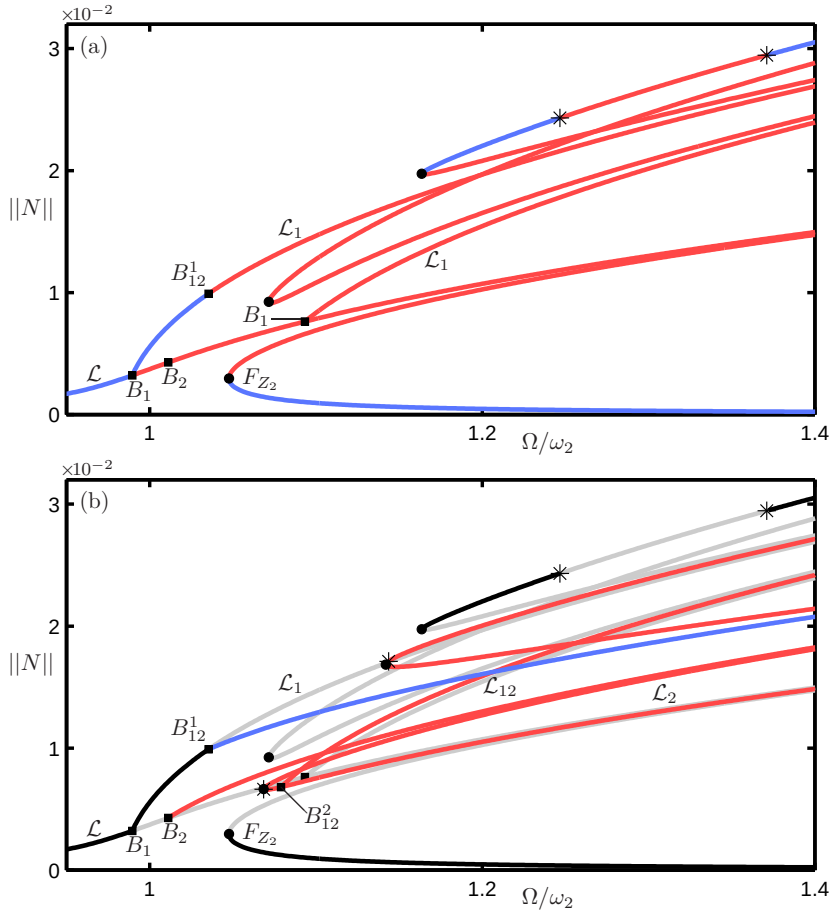

FIG. 14. *One-parameter bifurcation diagram in the* $(\Omega/\omega_2, ||N||)$*-plane for* $\Delta/L = 6.3 \times 10^{-4}$*. Panel (a) shows only the branches* $\mathcal{L}$ *and* $\mathcal{L}_1$*, and in panel (b) the branches* $\mathcal{L}_2$ *and* $\mathcal{L}_{12}$ *(coloured) are added to* $\mathcal{L}$ *and* $\mathcal{L}_1$ *(black and grey).*

A direct comparison of the frequency responses for $\Delta/L = 7 \times 10^{-5}$ and for $\Delta/L = 6.3 \times 10^{-4}$ is shown in figure 15 in the smaller parameter range $\Omega/\omega_2 \in [0.98, 1.06]$, similar to the one that we considered before, for example, in figure 10. In figure 15(a) for $\Delta/L = 7 \times 10^{-5}$ we find, for increasing Ω/ω_2 the response sequence $\mathcal{L}$ to $\mathcal{L}_2$ to $\mathcal{L}_{12}$ and back to $\mathcal{L}$, and vice versa with a hysteresis loop for decreasing Ω/ω_2. For $\Delta/L = 6.3 \times 10^{-4}$ in figure 15(b), on the other hand, we find for increasing Ω/ω_2 the response sequence $\mathcal{L}$ to $\mathcal{L}_1$ to $\mathcal{L}_{12}$, with the (Z_2, Y_1, Y_2)-mode being always observed for large Ω/ω_2. Starting from the Z_2-mode on the stable part of $\mathcal{L}$ for large and then decreasing Ω/ω_2, we find a transition at F_{Z_2} to the response sequence $\mathcal{L}_{12}$ to $\mathcal{L}_1$ to $\mathcal{L}$.

Overall, figures 3(b) and 15 show that the frequency response of the cable is very sensitive to even small changes of the excitation amplitude Δ/L. This a strong indication of the nonlinear nature of the coupling between the basic in-plane mode (represented by Z_2) and the two basic out-of plane modes (represented by Y_1 and Y_2).

4. Conclusions. We presented a bifurcation study of an inclined cable with support excitation near a 2 : 1 resonance with the second in-plane mode of the cable. This system was described by an ODE model for the contributions of this directly excited in-plane mode and of the first and second

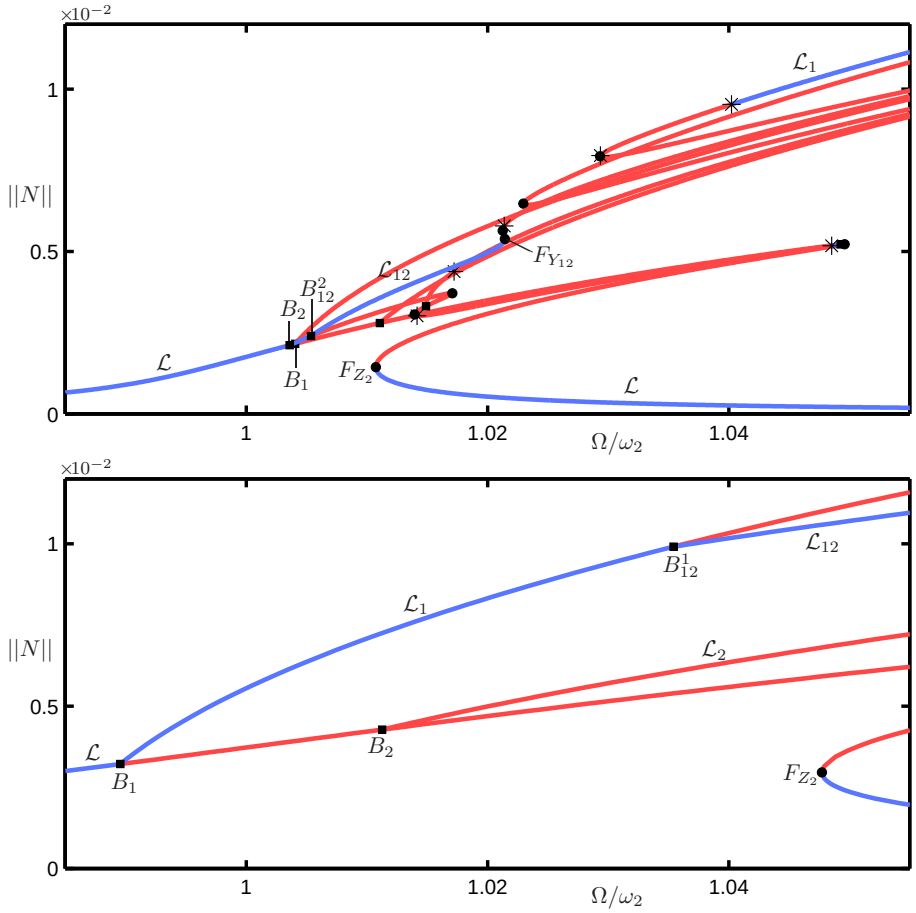

FIG. 15. *The one-parameter bifurcation diagrams in the* $(\Omega/\omega_2, ||N||)$*-plane for* $\Delta/L \approx 7 = 10^{-5}$ *in panel (a), and for* $\Delta/L = 6.3 \times 10^{-4}$ *in panel (b).*

out-of-plane modes of the cable. The focus was on the different types of coupled-mode response of the cable, which are equilibria of the ODE that are distinguished by which of the out-of-plane modes is active: none, the first, the second, or both. Each of the four types of equilibria was computed by means of numerical continuation as a surface in the three-dimensional space of their norm versus the amplitude and frequency of the excitation. The different surfaces connect at curves of bifurcations and constitute a geometric picture of the overall two-parameter bifurcation diagram of the coupled-mode response of the cable. The quite intricate structure of this bifurcation diagram confirms the nonlinear nature of the problem. In particular, we found that the frequency response of the cable depends very sensitively on the excitation amplitude.

An interesting subject for future research is the study of periodic orbits that bifurcate from Hopf bifurcations of the coupled modes. Physically, they correspond to a cable response with periodically varying amplitudes of the contributing basic in-plane and out-of-plane modes, which manifests itself in locked or quasiperiodic two-frequency dynamics. Initial investigations show that these periodic orbits of the model equations may bifurcate further, for example, in period-doubling and homoclinic bifurcations, which lead to a chaotic cable response. A systematic study of these cable dynamics with non-constant amplitudes of the basic modes is under way and will be reported

elsewhere.

The results we presented are for a range of the excitation frequency (close to the 2 : 1 resonance) where the first in-plane mode is not active and, therefore, the three-mode model considered here provides a suitable description of the cable response. Previously this model was studied in [9] mainly in terms of the stability properties of the pure in-plane response, and good agreement was found with the corresponding experiment. Similar experiments are reported in [15] for a longer cable, where again there was good agreement between measurements and the stability boundaries of in-plane motion. These results were obtained for a four-mode model that includes the first in-plane mode; however, the stability boundaries agree with those of the three-mode model for sufficiently small frequency detunings. It appears feasible for these reasons that the other cable responses predicted here, to which the out-of-plane modes contribute, may also be confirmed experimentally. Note, however, that such experiments are not straightforward, because the cable is only very lightly damped. Hence, experimental runs require a long time for transients to die down sufficiently before the dynamics can be recorded reliably (e.g., with video-capture at the half- and quarter-points).

Finally, we mention that in a cable-stayed bridge the cable dynamics may also have an influence on the bridge deck under certain conditions. The study presented here shows that the motion of the cable itself, under uni-directional excitation from the deck, may develop considerable amplitudes. Hence, there is the potential for positive feedback loops between vibrations of the cable and the deck. One approach to study such effects is to extend the model for the cable by adding one or more damped oscillators that model the basic modes of the bridge deck. This type of system could be studied in a similar spirt via a bifurcation analysis of the coupled-mode responses of the overall system, which now also include the basic deck modes.

Acknowledgements. The research of V.T. was supported by grant EP/F030711/1 from the Engineering and Physical Sciences Research Council (EPSRC).

REFERENCES

[1] T. Bakri, R. Nabergoj, A. Tonel, F. Verhulst, Parametric excitation in non-linear dynamics. *International Journal Non-linear Mechanics*, 39 (2004) 311–329.

[2] A. Berlioz, C.H. Lamarque, A non-linear model for the dynamics of an inclined cable. *Journal of Sound and Vibration*, 279(3-5) (2005) 619–639.

[3] E.J. Doedel, with major contributions from A.R. Champneys, T.F. Fairgrieve, Yu.A. Kuznetsov, B.E. Oldeman, R.C. Paffenroth, B. Sandstede, X.J. Wang, and C. Zhang. *AUTO2000 and AUTO-07P: Continuation and bifurcation software for ordinary differential equations*, Department of Computer Science, Concordia University, Montreal, Canada, 2000; available from `http://sourceforge.net/projects/auto2000`.

[4] E.J. Doedel, in *Numerical Continuation Methods for Dynamical Systems*, edited by B. Krauskopf, H.M. Osinga, and J. Galán-Vioque, Springer-Verlag, Dordrecht, 2007.

[5] Y. Fujino, P. Warnitchai and B.M. Pacheco, An experimental and analytical study of autoparametric resonance in a 3DOF model of cable-stayed-beam. *Nonlinear Dynam.*, 4 (1993) 111–138.

[6] V. Gattulli, M. Lepidi, J.H.G. Macdonald and C.A. Taylor, One-to-two global local interaction in a cable stayed beam observed through analytical, finite element and experimental models. *International Journal of Non-Linear Mechanics*, 40(5) (2005) 571–588.

[7] V. Gattulli, L. Martinelli, F. Perotti, F. Vestroni, Non-linear oscillations of cables under harmonic loading using analytical and finite element models. *Comput. Meth. Appl. Mech. Eng.*, 193 (2004) 69–85.

[8] C.T. Georgakis, J.H.G. Macdonald, C.A. Taylor, Non-linear analysis of wind-induced cable-deck interaction. *IABSE Conference Cable-supported Bridges, Seoul, South Korea*, 2001, IABSE Reports, 84, Paper 330.

[9] A. Gonzalez-Buelga, S.A. Neild, D.J. Wagg, J.H.G. Macdonald, Modal stability of inclined cables subjected to vertical support excitation. *Journal of Sound and Vibration*, 318 (2008) 565–579.

[10] J. Guckenheimer, P. Holmes. *Nonlinear Oscillations, Dynamical Systems and Bifurcations of Vector Fields.* Springer-Verlag, New York/Berlin, second edition, 1986.

[11] H. Irvine, *Cable structures.* MIT Press, Cambridge, MA. 1981.

[12] Yu.A. Kuznetsov *Elements of Applied Bifurcation Theory.* Springer-Verlag, New York/Berlin, second edition, 1998.

[13] J.L. Lilien, A.P. Pinto Da Costa, Vibration amplitudes caused by parametric excitation of cable stayed structures. *Journal Sound and Vibration* 174 (1994) 69–90.

[14] J.H.G. Macdonald, M.S. Dietz, S.A. Neild, A. Gonzalez-Buelga, A.J. Crewe, D.J. Wagg, Generalised modal stability of inclined cables subjected to support excitations. *Journal of Sound and Vibration*, 329 (2010) 4515–4533.

[15] M.R. Marsico, V. Tzanov, D.J. Wagg, S.A. Neild, B. Krauskopf. Bifurcation analysis of a parametrically excited inclined cable close to two-to-one internal resonance. *Journal of Sound and Vibration*, 330 (2011) 6023–6035.

[16] A.H. Nayfeh, P.F. Pai, *Linear and Nonlinear Structural Mechanics*. Wiley, 2004.

[17] O. O'Reilly, P. Holmes. Non-linear, non-planar and non-periodic vibrations of a string. *Journal of Sound and Vibration*, 153(3) (1992) 413–435.

[18] G. Rega, Nonlinear vibrations of suspended cables- part i: Modeling and analysis. *Applied Mechanics Review*, 57 (2004) 443–478.

[19] G. Rega, Nonlinear vibrations of suspended cables- part ii: Deterministic phenomena. *Applied Mechanics Review* 57 (2004) 479–514.

[20] G. Rega, R. Alaggio, F. Benedettini, Experimental Investigation of the Nonlinear Response of a Hanging Cable. Part I: Local Analysis. *Nonlinear Dynamics*, 17 (1997) 89–117.

[21] G. Rega, R. Alaggio, Experimental unfolding of the nonlinear dynamics of a cable-mass suspended system around a divergence-Hopf bifurcation. *Journal of Sound and Vibration*, 322 (2009) 581–611.

[22] G. Rega, W. Lacarbonara, A.H. Nayfeh, C.M. Chin, Multiple resonances in suspended cables: direct versus reduced-order models. *International Journal of Non-linear Mechanics*, 34(5) (1999) 901–924.

[23] G. Rega, N. Srinil, R. Alaggio, Experimetal and Numerical Studies of Inclined Cables: free and parametrically-forced vibrations. *Journal of Theoretical and Applied Mechanics*, 3(46) (2008) 621–640.

[24] N. Srinil, G. Rega, Two-to-one resonant multi-modal dynamics of horizontal/inclined cables. part ii: Internal resonance activation, reduced-order models and nonlinear normal modes. *Nonlinear Dynamics*, 48(3) (2007) 253–274.

[25] N. Srinil, G. Rega, S. Chucheepsakul, Three-dimensional non-linear coupling and dynamic tension in the large-amplitude free vibrations of arbitrarily sagged cables. *Journal of Sound and Vibration*, 269(3-5) (2004) 823–852.

[26] N. Srinil, G. Rega, S. Chucheepsakul, Two-to-one resonant multi-modal dynamics of horizontal/inclined cables. part i: Theoretical formulation and model validation. *Nonlinear Dynamics*, 48(3) (2007) 231–252.

[27] G. Tagata, Harmonically forced, finite amplitude vibration of a string. *Journal of Sound and Vibration* 51 (4) (1977) 483492.

[28] V. Tzanov, M. R. Marsico, D.J. Wagg, B. Krauskopf, S.A. Neild, Internal resonance between in-plane and out-of-plane modes of vibration of inclined cables subjected to vertical support excitation. *Proceedings of EURODYN 2011, 8-th International Conference on Structural Dynamics.*

[29] V. Tzanov, S.A. Neild, B. Krauskopf, D.J. Wagg, Influence of damping on the vibration of an inclined cable subjected to support excitation. *Proceedings of ASME 2011 Design Engineering technical Conference and Computers and Information in Engineering Conference.*

[30] R. Uhrig, On kinetic response of cables of cable-stayed bridges due to combined parametric and forced excitation. *Journal of Sound and Vibration* 165 (1) (1993) 185192.

[31] F. Verhulst, *Nonlinear Differential Equations and Dynamical Systems*. Springer-Verlag, 1996.

[32] D.J. Wagg, S.A. Neild, *Nonlinear Vibration with Control*. Springer-Verlag, 2010.

[33] P. Warnitchai, Y. Fujino, T. Susumpow, A nonlinear dynamic model for cables and its application to a cable structure system. *Journal of Sound and Vibration*, 187(4) (1995) 695–712.